Published OnlineFirst May 22, 2020; DOI: 10.1158/2159-8290.CD-19-1436

RESEARCH ARTICLE

Posttranslational Regulation of the Exon Skipping Machinery Controls Aberrant Splicing in Leukemia

Yalu Zhou[1,2], Cuijuan Han[1,2], Eric Wang[3], Adam H. Lorch[1,2], Valentina Serafin[4], Byoung-Kyu Cho[5], Blanca T. Gutierrez Diaz[1,2], Julien Calvo[6,7], Celestia Fang[1,2,8], Alireza Khodadadi-Jamayran[9], Tommaso Tabaglio[10,11], Christian Marier[12], Anna Kuchmiy[13,14], Limin Sun[1,2], George Yacu[1,2], Szymon K. Filip[5], Qi Jin[1,2], Yoh-Hei Takahashi[1,2], David R. Amici[1,2,8], Emily J. Rendleman[1,2], Radhika Rawat[1,2,8], Silvia Bresolin[4], Maddalena Paganin[4], Cheng Zhang[15], Hu Li[15], Irawati Kandela[16], Yuliya Politanska[17], Hiam Abdala-Valencia[17], Marc L. Mendillo[1,2], Ping Zhu[18], Bruno Palhais[13,19], Pieter Van Vlierberghe[13,19], Tom Taghon[13,14,20], Iannis Aifantis[3], Young Ah Goo[1,5], Ernesto Guccione[21,22], Adriana Heguy[3,12], Aristotelis Tsirigos[3,9], Keng Boon Wee[10,11], Rama K. Mishra[1,23], Francoise Pflumio[6,7], Benedetta Accordi[4], Giuseppe Basso[4], and Panagiotis Ntziachristos[1,2,24]

ABSTRACT

Splicing alterations are common in diseases such as cancer, where mutations in splicing factor genes are frequently responsible for aberrant splicing. Here we present an alternative mechanism for splicing regulation in T-cell acute lymphoblastic leukemia (T-ALL) that involves posttranslational stabilization of the splicing machinery via deubiquitination. We demonstrate there are extensive exon skipping changes in disease, affecting proteasomal subunits, cell-cycle regulators, and the RNA machinery. We present that the serine/arginine-rich splicing factors (SRSF), controlling exon skipping, are critical for leukemia cell survival. The ubiquitin-specific peptidase 7 (USP7) regulates SRSF6 protein levels via active deubiquitination, and USP7 inhibition alters the exon skipping pattern and blocks T-ALL growth. The splicing inhibitor H3B-8800 affects splicing of proteasomal transcripts and proteasome activity and acts synergistically with proteasome inhibitors in inhibiting T-ALL growth. Our study provides the proof-of-principle for regulation of splicing factors via deubiquitination and suggests new therapeutic modalities in T-ALL.

SIGNIFICANCE: Our study provides a new proof-of-principle for posttranslational regulation of splicing factors independently of mutations in aggressive T-cell leukemia. It further suggests a new drug combination of splicing and proteasomal inhibitors, a concept that might apply to other diseases with or without mutations affecting the splicing machinery.

[1]Department of Biochemistry and Molecular Genetics, Northwestern University, Chicago, Illinois. [2]Simpson Querrey Institute for Epigenetics, Northwestern University Feinberg School of Medicine, Chicago, Illinois. [3]Department of Pathology and Laura & Isaac Perlmutter Cancer Center, New York University School of Medicine, New York, New York. [4]Oncohematology Laboratory, Department of Women's and Children's Health, University of Padova, Padova, Italy. [5]Proteomics Center of Excellence, Northwestern University, Evanston, Illinois. [6]Team Niche and Cancer in hematopoiesis, CEA, Fontenay-aux-Roses, France. [7]Laboratory of Hematopoietic Stem Cells and Leukemia/Service Stem Cells and Radiation/iRCM/JACOB/DRF, CEA, Fontenay-aux-Roses, France. [8]Medical Scientist Training Program, Northwestern University Feinberg School of Medicine, Chicago, Illinois. [9]Applied Bioinformatics Laboratories, Office of Science and Research, New York University School of Medicine, New York, New York. [10]Institute of Molecular and Cell Biology, Agency for Science, Technology and Research, Singapore. [11]Department of Biochemistry, Yong Loo Lin School of Medicine, National University of Singapore, Singapore. [12]Genome Technology Center, New York University School of Medicine, New York, New York. [13]Cancer Research Institute Ghent (CRIG), Ghent, Belgium. [14]Department of Diagnostic Sciences, Ghent University, Ghent, Belgium. [15]Department of Molecular Pharmacology and Experimental Therapeutics, Mayo Clinic, Rochester, Minnesota. [16]Center for Developmental Therapeutics, Northwestern University, Evanston, Illinois. [17]Department of Medicine, Northwestern University Feinberg School of Medicine, Chicago, Illinois.

Published OnlineFirst May 22, 2020; DOI: 10.1158/2159-8290.CD-19-1436

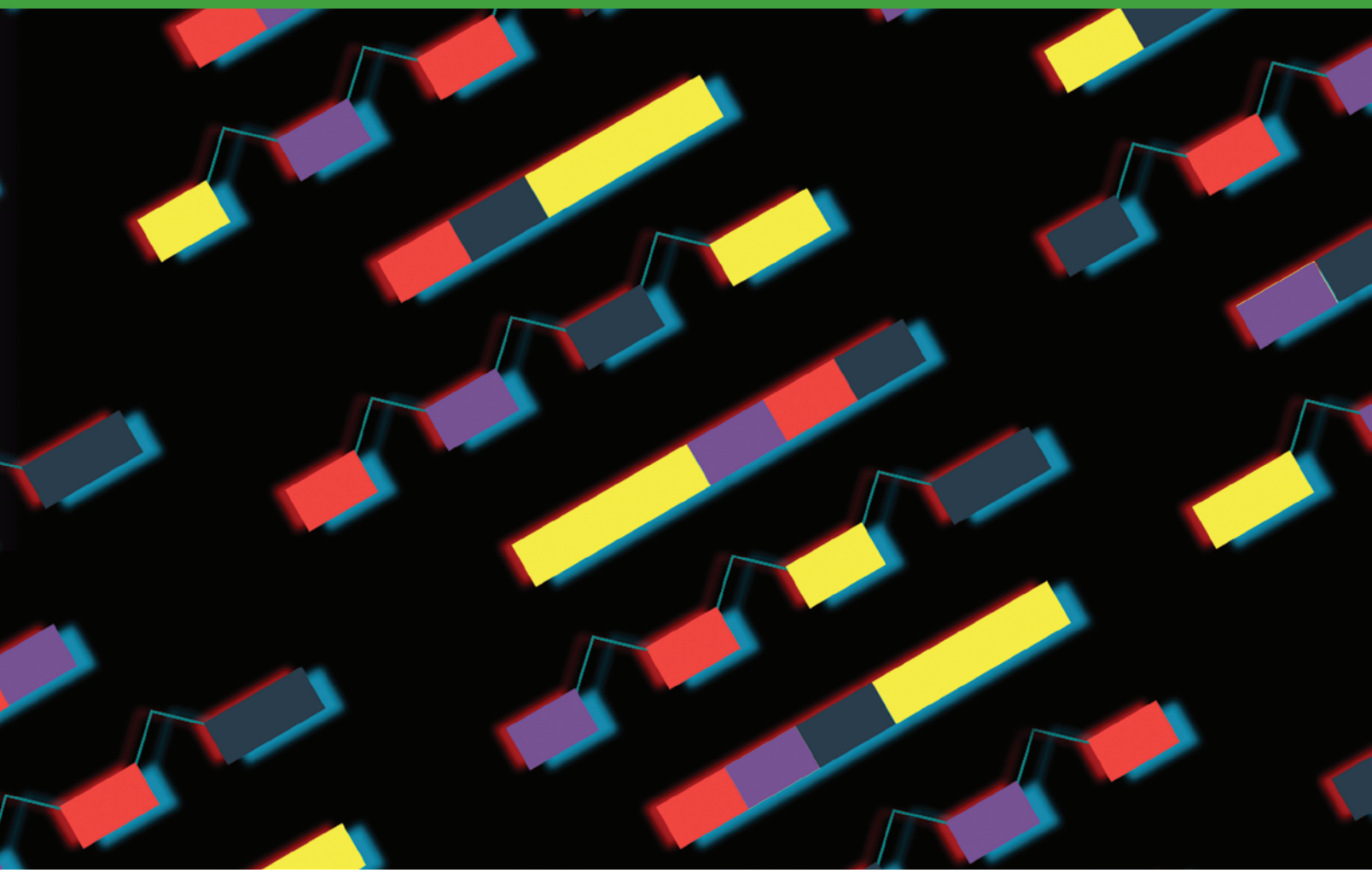

INTRODUCTION

Alternative splicing is a critical mechanism of posttranscriptional regulation that is mediated by the ribonucleoprotein complex commonly known as the spliceosome. It is estimated that more than 90% of transcripts from multiexonic protein-coding transcripts could be alternatively spliced in a tissue- or developmental stage–specific manner, under stress or in disease (1). Whereas the average human gene produces three or more alternatively spliced mRNA isoforms, malignant cells produce a significant surplus of splice variants. These atypical splice variants appear to be products of missplicing that in many cases are secondary to either mutations in splicing factors or dysregulation of their expression. The prevalence of these anomalies in the splicing machinery is elevated in certain types of hematologic malignancies and provides a unique opportunity for therapeutic targeting (2–4).

The splicing machinery is frequently mutated in the early stages of many types of cancer, such as myelodysplastic syndromes or chronic lymphocytic leukemia, demonstrating the importance of this pathway for cellular function (2–13). Aberrant splicing is mostly attributed to genetic alterations affecting the splicing factor genes. These mutations occur most commonly in splicing factor 3b subunit 1 (*SF3B1*), serine/arginine-rich splicing factor 2 (*SRSF2*), zinc finger RNA binding motif and serine/arginine rich 2 (*ZRSR2*), and U2 small nuclear RNA auxiliary factor 1 (*U2AF1*) and in a mutually

[18]H3 Biomedicine, Inc., Cambridge, Massachusetts. [19]Department of Biomolecular Medicine, Ghent University, Ghent, Belgium. [20]Faculty of Medicine and Health Sciences, Ghent University, Ghent, Belgium. [21]Department of Oncological Sciences and Tisch Cancer Institute, Icahn School of Medicine at Mount Sinai, New York, New York. [22]Department of Pharmacological Sciences and Mount Sinai Center for Therapeutics Discovery, Icahn School of Medicine at Mount Sinai, New York, New York. [23]Center for Molecular Innovation and Drug Discovery, Northwestern University, Chicago, Illinois. [24]Robert H. Lurie Comprehensive Cancer Center, Northwestern University, Chicago, Illinois.

Note: Supplementary data for this article are available at Cancer Discovery Online (http://cancerdiscovery.aacrjournals.org/).

Corresponding Author: Panagiotis Ntziachristos, Northwestern University Feinberg School of Medicine, 303 East Superior Street, SQBR 7-304, Chicago, IL 60611. Phone: 347-703-0048; Fax: 312-503-4081; E-mail: pntziachr@gmail.com

Cancer Discov 2020;10:1–22

doi: 10.1158/2159-8290.CD-19-1436

Published OnlineFirst May 22, 2020; DOI: 10.1158/2159-8290.CD-19-1436

exclusive fashion, as mutations in more than one factor are lethal for tumor and normal cells alike (14). In addition, mutations affecting RNAs that are part of the spliceosome were recently identified (15). However, splicing abnormalities found in cancer are not always associated with mutations in these or related genes. Instead, they may arise from aberrant expression of splicing factors (16–25). Certain serine/arginine-rich (SR) splicing factor proteins are overexpressed in human cancers, notably SRSF1 (16–19, 25), SRSF6 (16, 20, 21), and SRSF3 (22–24). Part of this activation might be due to gene amplification as well as transcriptional regulation, mainly through MYC. Expression-related variations in splicing are mostly observed in solid tumors of adult origin, suggesting a potential explanation for differences in splicing biology between solid and blood-based cancers.

Acute lymphoblastic leukemia (ALL) is an aggressive pediatric and adult type of leukemia of T and B cell origin, translating to approximately 3,100 children and adolescents diagnosed with the disease each year in the United States. T-cell ALL (T-ALL) is driven by the hyperactivation of pathways such as NOTCH1 (26–31), and the incidence of this disease subtype is increasing (32). One fifth of pediatric patients and more than 50% of adult patients with T-ALL do not achieve a complete remission or they relapse after consolidated chemotherapy, making resistance to therapy the most substantial challenge in disease treatment (30, 33, 34). T-ALL is an epigenetic disease presenting with deregulation of epigenetic enzymes. As many T-ALL oncogenes are transcription factors, disease initiation and progression are coordinated via epigenetic regulators in the cell nucleus. Work by our lab and others has described the major epigenetic players in this disease (26, 27, 35–46). However, the design of treatment strategies based on direct inhibitors of these proteins has been challenging, as oncogenes such as NOTCH1 are broadly involved in physiologic processes. Furthermore, there are very few documented mutations affecting splicing factors in T-ALL (47), and the splicing landscape in T-ALL is relatively poorly characterized. Thus, as of this writing, we lack evidence-based strategies for treating cancers such as T-ALL that have no or very few splicing factor mutations. In addition, mechanisms of resistance in T-ALL remain poorly characterized due to the absence of appropriate leukemia models and needed technologies.

Although we and others have previously demonstrated the role of epigenetic factors and oncogenic long noncoding RNAs in T-ALL (40–42), the role of aberrant splicing and mechanisms of abnormal posttranslational regulation of the splicing machinery in T-ALL progression have been relatively uncharacterized. In this study, we sought to characterize splicing alterations in T-ALL, potential mechanisms regulating aberrant splicing, and their implications for T-ALL biology.

RESULTS

T-ALL Is Characterized by Significant Splicing Changes Compared with Physiologic T Cells

To characterize the splicing landscape in different types of human peripheral CD3$^+$ (CD4$^+$/CD8$^+$) T cells, in comparison with 3 patients with T-cell leukemia, we performed paired-end sequencing of the transcriptome to cover the splicing junctions. To study any T cell subtype–specific and differentiation stage–specific phenomena, we also included a T-cell subtype, CD4$^+$ T cells, and undifferentiated fast-proliferating thymocytes. Initial expression analysis of normal and tumor samples using edgeR (48) showed a significant upregulation of oncogenic targets in T-ALL, including NOTCH1 targets, as well as cell-cycle regulators, in agreement with previous findings in human and mouse contexts of T-ALL (ref. 40; Fig. 1A; Supplementary Fig. S1A–S1D; Supplementary Tables S1–S3). We then used rMATS (49), an established method for quantitative analysis of differential splicing phenomena, to cluster splicing changes between peripheral CD3$^+$ T cells and T-ALL in five distinct categories: exon skipping, intron retention, mutually exclusive exons, and usage of alternative 3′ or alternative 5′ splice sites (Fig. 1B; Supplementary Fig. S1E). We observed changes for each of these splicing categories between the two cell populations, with the most extensive splicing changes affecting skipped exons and retained introns (Fig. 1B and C; Supplementary Figs. 1E, S2A, and S2B). Overall, there was a significant increase in exon skipping events in T-ALL cells compared with normal T cells (see

Figure 1. Extensive changes in exon-skipping phenomena in T-ALL compared with physiologic T cells. **A,** Heat map of gene expression changes representing 630 significantly upregulated genes and 531 downregulated genes in T-ALL patient samples compared with CD3$^+$ T cells, ranked on the basis of expression level in T-ALL ($n = 3$; adj. $P < 0.01$). **B,** Differential splicing in T-ALL versus CD3$^+$ T cells. Bar graph (left) represents different types of splicing events; pie chart (right) shows T-ALL–specific splicing phenomena (corresponding to the gray bars). The plot represents the MATS analysis using three biological replicates per group. Only events that passed the statistics threshold (FDR < 0.05) and PSI > 0.1 (10% of the transcripts of a given gene) are taken into consideration. Exon skipping (SE) is the type of event affected most significantly. A3SS, alternative 3′ splice sites; A5SS, alternative 5′ splice sites; MXE, mutually exclusive exons; RI, intron retention. **C,** Directionality of exon skipping in T-ALL compared with T-cell subtypes, where positive (blue) and negative (red) values represent exon inclusion and exclusion, respectively. Please note there is a higher number of skipped exons in T-ALL (red) compared with any T-cell subtype. **B** and **C** collectively show that there are more skipped exons in T-ALL compared with normal T cells. **D,** Overlapping transcripts affected by splicing changes in T-ALL compared with CD3$^+$ T cells, CD4$^+$ T cells, and thymocytes (*FDR* < 0.05). **E,** Kyoto Encyclopedia of Genes and Genomes (KEGG) analysis showing main transcript pathways enriched in overlapped splicing events between T-cell subtypes and T-ALL from **D**. Transcript categories are ranked on the basis of enrichment score, *P* value, and size of the group. **F,** Scatter plot of splicing changes and distribution in T-ALL compared with CD3$^+$ T cells. Selected transcripts are colored on the basis of the type of differentially spliced event. Transcripts presenting PSI > 0.1 are shown. **G,** *De novo* binding motif discovery based on exon skipping data (including the skipped exon and flanking intron/exon sequences) in T-ALL versus CD3$^+$ T cells using rMAPS. SRSF6-bound motif enrichment in skipped exons in T-ALL (red) and in included exons in CD3$^+$ T-cells (in blue) is shown. Background motif enrichment is shown in black and −log (*P*) over the background is represented by red and blue dotted lines. **H,** Relative essentiality of the SRSF gene family across different types of cancer cell lines. Essentiality data, reflecting the importance of individual genes for cellular fitness, was obtained from the Project Achilles CRISPR/Cas9 screening dataset of 563 cancer cell lines. **I,** Essentiality for SRSF6 among different cancer types from the Project Achilles. A gene essentiality score of 1 is typical for genes considered pan-essential, such as ribosome components. T-ALL and other representative cancer types are shown. B-ALL, B cell acute lymphoblastic leukemia; TNBC, triple-negative breast cancer; AML, acute myeloid leukemia.

Published OnlineFirst May 22, 2020; DOI: 10.1158/2159-8290.CD-19-1436

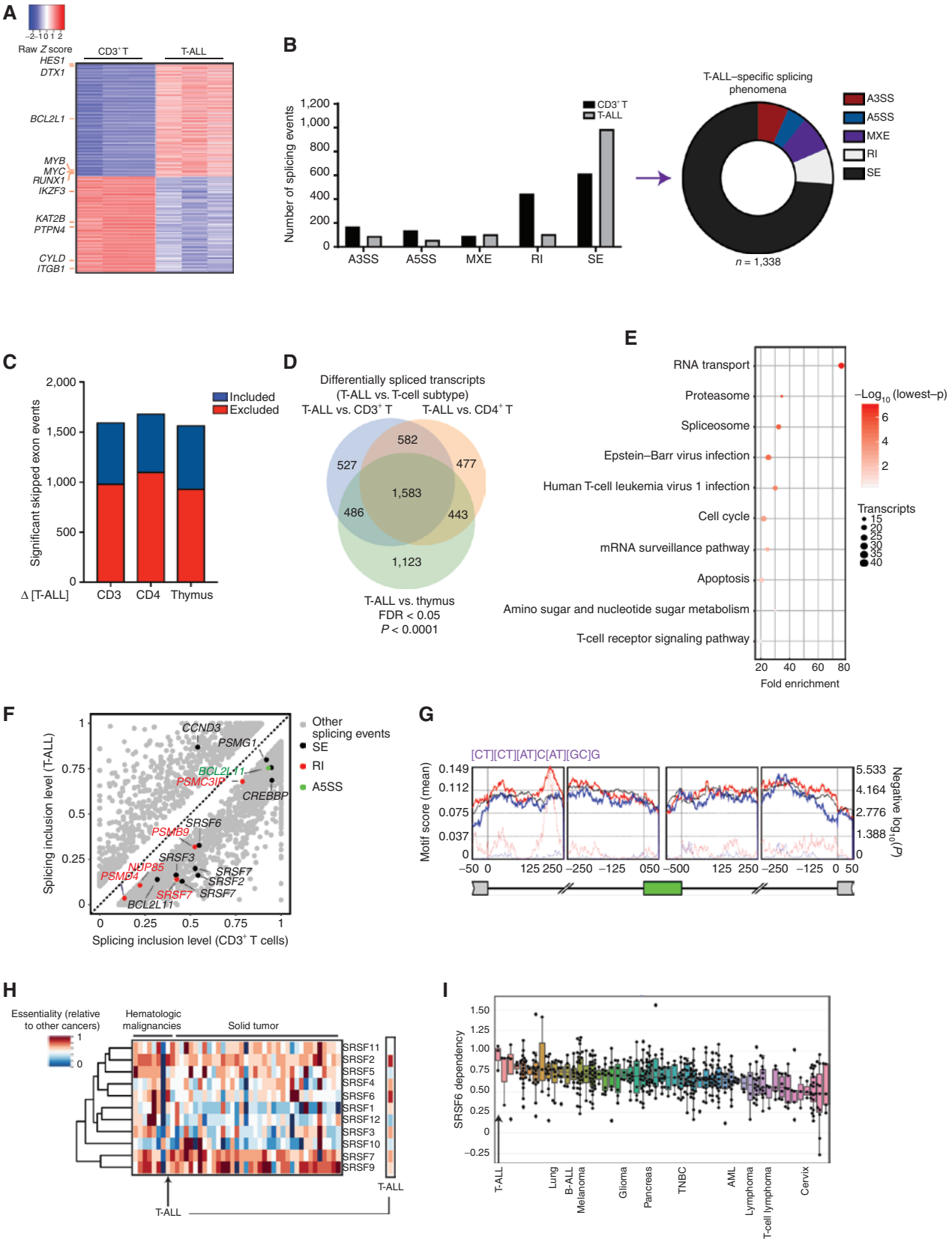

Published OnlineFirst May 22, 2020; DOI: 10.1158/2159-8290.CD-19-1436

red bar representing excluded exons, Fig. 1C). An alternative analysis quantifying exon inclusion levels and comparison of normal T-cell subsets with patients with T-ALL showed there are more exon inclusion phenomena in T cells compared with T-ALL (Supplementary Fig. S2C). In conclusion, T-cell cancers present with a higher number of skipped exon phenomena compared with physiologic T cells.

By performing a transcript-based analysis, we identified a total of 1,583 alternatively spliced transcripts in T-ALL compared with all three physiologic T-cell subsets [Fig. 1D, false discovery rate (FDR) < 0.05]. We noticed significant changes in spliceosome and RNA transport–related transcripts (Fig. 1E; Supplementary Table S4). We also report extensive changes in proteasome, apoptosis, and cell-cycle–related transcripts (Fig. 1E; Supplementary Table S4). More comprehensive splicing analysis in T-cell subsets showed extensive similarities with each other and differences when compared with T-ALL (Supplementary Fig. S2D). We further compared the different T-cell subsets to show that splicing phenomena reflect their developmental stages; differentiated $CD4^+$ cells present 1,668 alternatively regulated splicing events compared with $CD3^+$ T cells and 3,129 alternatively regulated splicing events compared with undifferentiated thymocytes (Supplementary Fig. S2E). These differences in splicing between T-cell subtypes potentially recapitulate biological characteristics (ref. 50; Supplementary Fig. S2F). For instance, faster proliferation is a major difference between T-cell progenitors in the thymus and terminally differentiated T cells. Indeed, Kyoto Encyclopedia of Genes and Genomes (KEGG) analysis of thymocyte-specific splicing phenomena showed that cell-cycle transcripts are differentially spliced between differentiated $CD3^+$ and $CD4^+$ cells and thymocytes (Supplementary Fig. S2G; Supplementary Table S5). Our findings suggest that the splicing landscape recapitulates lineage- or development-related biological characteristics.

We then performed further filtering based on the "percent spliced in" [PSI, or splicing inclusion level, 0 (0%) to 1 (100%); ref. 1] value changes between T-cell subsets and T-ALL, after normalizing all transcripts belonging to a specific isoform or alternatively spliced sequence of interest relative to all transcripts of the gene. In this case, we consider significant only changes bigger than 10% or PSI > 0.1. Focusing on transcript categories enriched in our enrichment analysis, we identified alternative splicing events affecting RNA transportation (e.g., NUP85), proteasomal-related transcripts (e.g., *PSMG1, PSMB9, PSMD4, PSMC3IP*), cell-cycle transcripts (*CCND3*), epigenetic enzymes (*CREBBP* or *CBP*), and apoptotic factors [BCL2L11; Fig. 1F (for $CD3^+$ T cells vs. T-ALL)]. Spliceosome components were also enriched in the differentially spliced transcripts, with a particular enrichment for serine/arginine-rich splicing factor (SRSF) transcript family (e.g., *SRSF2, SRSF3, SRSF6, SRSF7*). We noticed a similar enrichment in alternatively spliced spliceosome, proteasome, and RNA biology–related transcripts under more stringent conditions as well (PSI > 0.2, Supplementary Fig. S3A and S3B). We then sought out to confirm splicing changes affecting exon skipping and intron retention in SRSF factors (Supplementary Fig. S3C). SRSF levels are controlled via a process called nonsense-mediated decay (NMD), where transcripts containing a premature termination codon are degraded by the cellular machinery coordinated via binding of the regulator of nonsense transcripts 1 (UPF1). The *SRSF6* NMD allele contains exon 3 (poison exon) that, in turn, contains a termination codon (51, 52). We detect exon 3 in T-cell samples, and we show it is skipped in T-ALL (Supplementary Fig. S3C and S3D). In addition, silencing of *UPF1* in leukemia cells led to a slight but significant increase of the *SRSF6* NMD allele (Supplementary Fig. S3E–S3G). These results provide evidence for regulation of the *SRSF6* transcript levels via NMD in T cells. An unbiased *de novo* motif analysis using the rMAPS2 Motif Map (53) using exon skipping–associated areas between $CD3^+$ T cells and T-ALL identified the previously characterized SRSF6-bound sequence (21) as the top motif in the exon–intron junction upstream of the skipped exon (in purple, Fig. 1G; Supplementary Table S6), suggesting a potential role for SRSF6 in controlling exon skipping in T-ALL.

We next sought to map splicing changes in T-ALL cases that do not respond to chemotherapy or that relapse ["high-risk" (HR)], which represent the main therapeutic unmet need in T-ALL. This risk of disease relapse is determined on the basis of the detection (HR) or not ["non–high-risk" (NHR) disease] of residual cancer cells on day 35 from initiation of chemotherapy treatment. We sequenced 4 HR and 10 NHR diagnostic samples to validate splicing changes in T-ALL. Using this new patient group (validation cohort), we initially confirmed that there are more exon skipping events in T-ALL cells compared with normal cells (Supplementary Fig. S4A and S4B). We show that similar to what we presented in Supplementary Fig. S2C, analysis of this larger patient set shows that there is a significantly higher number of exon inclusion phenomena [exon inclusion levels (EIL)] in $CD3^+$ T cells compared with T-ALL (Supplementary Fig. S4A), and inversely an increased number of exon skipping phenomena in T-ALL affecting proteasome transcripts, as well as cell-cycle regulator and epigenetic enzyme–related transcripts (Supplementary Fig. S4B). We next compared splicing changes in patients with HR and NHR T-ALL, and saw a dramatic increase in exon skipping events and a decrease in mutually exclusive exon events in HR T-ALL compared with NHR (Supplementary Fig. S4C). Further transcript-based gene ontology analysis of the affected transcripts showed that alternative splicing phenomena are related to the chemotherapy resistance observed in HR cases, such as DNA damage response and DNA repair, as well as to spliceosome, the proteasome, cell cycle, and epigenetic regulators (Supplementary Fig. S4D; Supplementary Table S7). Exon skipping and mutually exclusive exon changes between T-ALL and T cells as well as between HR and NHR cases are a hallmark of altered function of SRSF proteins (17, 21).

Serine/Arginine-Rich Splicing Factor Levels Are Critical for T-ALL Cell Survival

Driven by the extensive number of exon skipping events in T-ALL, we sought to characterize the importance of individual SRSF proteins in T-ALL in an unbiased manner. To this end, we analyzed CRISPR/Cas9 screen data from the Cancer Dependency Map project (*DepMap*; https://depmap.org/portal/) using 563 cell lines (54) from solid and blood-based tumors, including three T-ALL cell lines (SUPT1, PF382, HSB2; Supplementary Table S8). These data show that T-ALL cells are sensitive to SRSF deletion, in comparison with other

Published OnlineFirst May 22, 2020; DOI: 10.1158/2159-8290.CD-19-1436

cancer types (Fig. 1H; Supplementary Fig. S5A–S5K). Strikingly, T-ALL is the cancer type that is the most sensitive to *SRSF6* deletion (Fig. 1I). We further performed an in-house type II CRISPR system screen in JURKAT cells using a custom 2,900 single-guide RNA (sgRNAs, ~6–8 per gene) library against 490 well-defined RNA-binding proteins (RBP; refs. 55–57), similar to previous studies (58–60). In this negative selection screen, depletion of specific sgRNAs in the cell population was assessed over time (57, 61). Individual sgRNA read counts were evaluated by next-generation sequencing using genomic DNA from cells on day 4 and day 20 posttransduction of cells with viruses expressing the sgRNA library. For a given gene, we measured the average fold change of relative abundance of all sgRNAs targeting the gene on days 4 and 20. This negative selection screen revealed a strong enrichment for 60 RBPs including 7 SRSF factors (SRSF1, 2, 3, 6, 7, 10, and 11) in the depleted cell population (Supplementary Fig. S5L; Supplementary Table S9). To study the extent to which SRSF6 levels associate with disease prognosis in human T-ALL, we analyzed expression data for the SRSF factors, aside from SRSF8, which is expressed at very low levels in T-ALL, coupled to survival data from the pediatric cancer genome project (PECAN), to show that *SRSF6* and *SRSF1* are the only SRSF members whose high expression associates with unfavorable disease prognosis in T-ALL (Supplementary Fig. S6A–S6K). The aforementioned findings reached via two independent CRISPR-based studies, the *DepMap* study and our CRISPR screen, as well as via patient survival data underline the importance of SRSF family members, and SRSF6 in particular, for acute leukemia survival.

SRSF Proteins Are Posttranslationally Regulated in T-ALL

As exon skipping and mutually exclusive exon phenomena could be a result of alterations in SRSF levels due to mutations, genetic amplification, transcriptional upregulation, or posttranslational regulation (3, 4, 21), we initially studied genetic alterations in *SRSF*s and selected splicing factor genes frequently altered in other types of cancer such as *SF3B1, U2AF1*, and *ZRSF2*, in CUTLL1 and JURKAT cell lines, as well as our cohort of diagnostic samples used in Fig. 1 and Supplementary Fig. S4. We performed targeted sequencing to identify that only JURKAT cells (SF3B1, Val1128Ile) and one patient sample (SRSF7, Asn17Tyr) exhibit mutations in the splicing machinery (Supplementary Table S10). In addition, analysis of a pediatric cohort of 264 patients with T-ALL from PECAN (47), as well as a cohort of adult T-ALL cases (62), showed a small percentage of T-ALL cases with splicing factor mutations (Supplementary Fig. S7A and S7B, left), in contrast to other cancers such as chronic lymphocytic leukemia (CLL) and myelodysplastic syndromes (MDS; Supplementary Fig. S7B, middle and right), which exhibit more frequent mutations in the splicing machinery (2–4, 11, 13, 63, 64). This suggests there might be other ways the splicing could go awry in T-ALL, including transcriptional and posttranslational regulation.

We then studied the transcriptional levels of SRSFs in the T-ALL transcriptome, using a previously published large T-ALL cohort (65) to demonstrate a significant increase of select *SRSF* transcripts, including SRSF6, in T-ALL compared with normal T cells (Supplementary Fig. S7C and S7D). It was previously shown that splicing components, including SRSF1, might be controlled by MYC (17, 18, 66) and that splicing inhibition might be a therapeutic approach in MYC-positive tumors (67). In addition, NOTCH1 has been shown to transcriptionally control the *SQH1* splicing factor in T-ALL (68). Both NOTCH1 and MYC are major oncogenes in T-ALL, and our group has previously shown that NOTCH1 recruits USP7 to chromatin to promote transcriptional activation of oncogenic targets (69). Nevertheless, inhibition of NOTCH1 and MYC activity in the human T-ALL cell line JURKAT using gamma secretase and bromodomain inhibitors, respectively, yielded very few changes in splicing factors in general, and no changes in SRSF6 levels (Supplementary Fig. S7E). These findings demonstrate that SRSFs might be regulated in alternative, both direct and indirect, ways in T-ALL.

Initially, assessment of protein levels for SRSF6 in T-ALL patient samples showed that it collectively exhibits a significantly higher expression in T-ALL (Fig. 2A and B), and also exhibits a significant positive correlation between SRSF6 and USP7 protein levels in T-ALL (Fig. 2C). To further study the relevance of SRSF6 protein levels and biology in human T-ALL patient samples, we performed an analysis of SRSF6 protein levels in T-ALL patient samples using reverse-phase protein array (RPPA) with 14 HR and 31 NHR samples. There is a significant upregulation of SRSF6 protein levels in aggressive HR versus NHR leukemia (Fig. 2D). In contrast to protein levels, the mRNA levels of *SRSF6* are not different in aggressive disease (HR) cases compared with nonaggressive (standard- and low-risk) T-ALL or among the different T-ALL subsets (Supplementary Fig. S7F and S7G).

As our group recently characterized the major pro-oncogenic role of the deubiquitinase USP7 in T-ALL (69, 70), we examined protein levels of SRSF6 in comparison with USP7 levels in this larger patient cohort of HR and NHR patients. Similar to Fig. 2C, we noticed that SRSF6 protein levels significantly correlate with USP7 levels (Fig. 2E). We then performed USP7 pulldown studies coupled to mass spectrometry analysis in JURKAT cells to characterize the USP7 interactome. We identified that USP7 interacts with select splicing factors, with SRSF 3, 6, 7, and 10 being among the most enriched interactors (Fig. 2F; Supplementary Table S11). These findings suggest that USP7 might control protein stabilization of SRSF6 via deubiquitination. To study the extent to which USP7 controls the ubiquitination levels of SRSF6, we screened for ubiquitination changes in the human proteome. We treated JURKAT cells with vehicle or USP7 inhibitor P5091 over a period of 24 hours followed by global pulldown of ubiquitinated lysine residues in lysine-glycine-glycine (KGG) moieties using equal input protein amounts of whole-cell extracts (Fig. 2G). Mass spectrometry analysis generated a list of 393 differentially ubiquitinated proteins (Supplementary Table S12). Gene ontology analysis showed a significant enrichment in RNA-binding proteins (Fig. 2H; Supplementary Table S13). To identify direct USP7 substrates in T-ALL, we assessed the convergence of the differentially ubiquitinated proteins upon treatment with P5091 with the USP7 interactome (see Fig. 2F) to identify 58 proteins as direct USP7 substrates (Supplementary Fig. S8A; Supplementary Table S13). Network analysis and gene ontology analysis of the convergent set showed a significant

Published OnlineFirst May 22, 2020; DOI: 10.1158/2159-8290.CD-19-1436

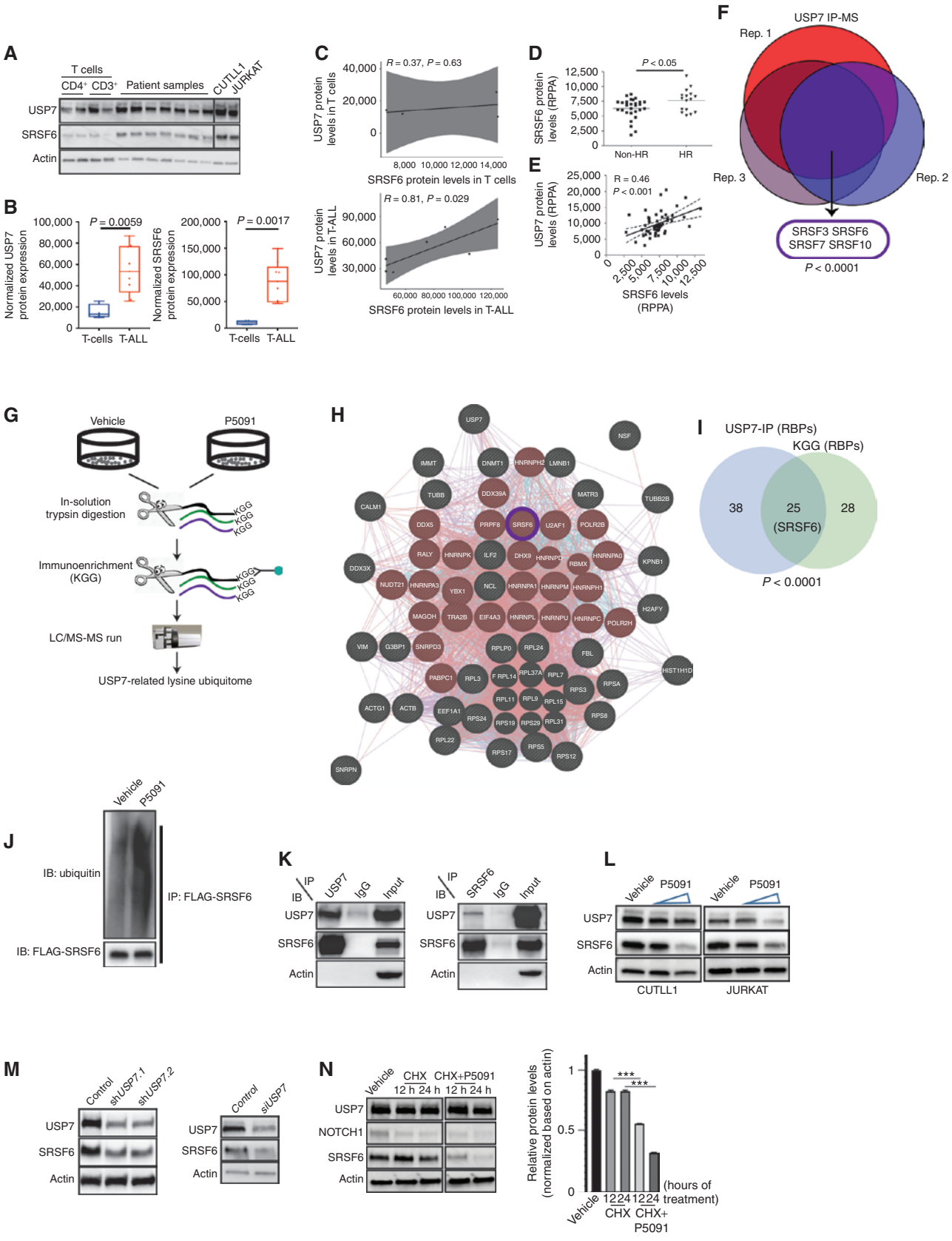

Published OnlineFirst May 22, 2020; DOI: 10.1158/2159-8290.CD-19-1436

enrichment of RNA-binding proteins such as the RNA-splicing machinery and RNA-metabolizing enzymes, including SRSF6, which presents with increased ubiquitination levels upon P5091 treatment ($n = 25$, Fig. 2H and I; Supplementary Fig. S8B; Supplementary Table S13). To further study USP7-mediated deubiquitination of SRSF6, we expressed FLAG-SRSF6 in CUTLL1 cells, coupled to treatment with vehicle or P5091, to test for changes in SRSF6 ubiquitination upon inhibition of USP7. Our results demonstrate the increase of SRSF6 ubiquitination upon P5091 treatment (Fig. 2J). To assess the importance of the catalytic activity of USP7 for the regulation of SRSF6 ubiquitination, we expressed SRSF6 and ubiquitin in the presence of wild-type catalytically active as well as catalytically deficient USP7 (USP7 CD). We show that there is a significant decrease in SRSF6 ubiquitination upon wild-type USP7, but not upon USP7 CD, expression (Supplementary Fig. S8C). As SRSF factors can be controlled at the posttranslational level via neddylation (71, 72), we further tested whether SRSF6 can be neddylated. Our studies showed that SRSF6 is not neddylated, in contrast to SRSF3, which presents with detectable levels of neddylation in agreement with previous studies (refs. 71, 72; Supplementary Fig. S8D). These studies suggest a role of the USP7 deubiquitinase activity in controlling SRSF6 protein levels.

We further validated the interaction between endogenous USP7 and SRSF6 proteins in JURKAT and CUTLL1 T-ALL cells by performing reciprocal immunoprecipitation experiments (Fig. 2K). To further test specificity of SRSF6 in T-ALL compared with potential roles other SRSF family members might play, we assayed for protein levels of SRSF3, another member of the SRSF family that also interacts with USP7 (Supplementary Fig. S8E). In contrast to SRSF6, we identified no difference in the SRSF3 levels between HR and NHR cases (Supplementary Fig. S8F). In addition, our studies did not yield detectable interactions of SRSF6 with other USP proteins such as UPS11 or USP47, which have been shown to interact and/or act together with USP7 (refs. 73–76; Supplementary Fig. S8G). SRSF6 consists of one RNA recognition motif (RRM) domain, one RRM homology (RRH) domain, and an arginine/serine-rich (RS) domain that mediates protein–protein interaction (Supplementary Fig. S8H). Studies using SRSF6 truncations showed that the RRH domain is required for SRSF6 interaction with USP7 (Supplementary Fig. S8H).

Inhibition of USP7 using the well-studied USP7 inhibitor P5091 (77) led to significant reduction of SRSF6 protein levels (Fig. 2L). Silencing of USP7 using short-hairpin RNA (shRNA) in CUTLL1 cells led to a decrease in SRSF6 protein levels similar to P5091 treatment, further underscoring the USP7-mediated regulation of SRSF6 (Fig. 2M, left). Treatment of 293T cells with siRNA against USP7 led to a similar reduction in SRSF6 protein levels suggesting a broader biological context for the regulation of SRSF6 by USP7 (Fig. 2M, right). Inhibition of global deubiquitinase activity using PR619 (78) also led to a significant downregulation of SRSF6 (Supplementary Fig. S8I), confirming regulation of SRSF6 from the deubiquitinase enzymes. We further show that proteasomal inhibition partially rescues the P5091-mediated reduction in SRSF6 levels (Supplementary Fig. S8J). Additional studies showed that inhibition of NOTCH1 or bromodomain proteins (i.e., MYC) did not affect SRSF6 protein levels (Supplementary Fig. S8K). Gel filtration analysis suggested that SRSF6 might form a complex with USP7 distinct from the USP7 and SF3B1 complex (Supplementary Fig. S8L), suggesting potential participation of USP7 in different splicing complexes.

Gene expression analysis of splicing transcripts in T-ALL cells upon treatment with P5091 showed downregulation of SRSF transcripts encoding for SRSF proteins and SRSF6 in particular (Supplementary Fig. S8M and S8N). To differentiate between a potential impact of USP7 in transcriptional versus posttranslational regulation of SRSF6, we treated CUTLL1 cells with cycloheximide to block translation in the presence or absence of P5091. Analysis of SRSF6 levels showed that the combination of cycloheximide and P5091 treatment leads to a faster decrease in SRSF6 levels compared with cycloheximide alone, suggesting USP7 controls protein levels of SRSF6 irrespective of potential effects on *SRSF6* gene transcription (Fig. 2N).

SRSF6 Levels Are Critical for Leukemia Growth

We then sought to test the role of SRSF6 as an important USP7 substrate. We ectopically expressed SRSF6 in CUTLL1 cells coupled to treatment with vehicle or P5091 USP7 inhibitor. We showed that overexpression of SRSF6 in T-ALL cells leads to a partial rescue of growth inhibition caused by P5091 (Supplementary Fig. S9A). This shows that SRSF6 protein is a biologically relevant substrate of USP7. To confirm this conclusion, we performed genomic silencing of USP7, which

Figure 2. Posttranslational regulation of SRSF6 by USP7. **A,** Immunoblot showing SRSF6 protein levels in normal CD4$^+$ T-cells ($n = 2$) and CD3$^+$ T cells ($n = 2$), patients with T-ALL ($n = 7$), and CUTLL1 and JURKAT cells. **B** and **C,** Quantification of immunoblot bands presented in **A**. USP7 and SRSF6 protein levels are higher in T-ALL compared with T cells (**B**). USP7 protein levels significantly correlate with SRSF6 levels in T-ALL (**C**). Actin is used as a loading control. **D** and **E**, RPPA analysis for SRSF6 protein levels in HR ($n = 16$) versus non-HR T-ALL ($n = 31$) cases (**D**) and correlation with USP7 expression (**E**). **F,** USP7 immunoprecipitation coupled to mass spectrometry (IP-MS) analysis in JURKAT cells. Shown is the overlap of USP7-associated proteins across three biological replicates, revealing splicing factors associated with USP7. **G,** Schematic representation of the USP7-related lysine ubiquitome analysis in JURKAT cells. **H,** Network analysis of the overlapped proteins of USP7 IP-MS and KGG mass spectrometry using GeneMANIA. Splicing related proteins are highlighted in red. **I,** Analysis of the overlapping datasets for USP7 IP-MS and KGG mass spectrometry studies reveals a significant number of RNA binding proteins in common (25; $P < 0.0001$). **J,** Immunoblot for detection of ubiquitination upon lentiviral expression of FLAG-tagged SRSF6 in CUTLL1 cells coupled to treatment with P5091. The FLAG epitope was used for SRSF6 pulldown. A representative blot for one biological replicate of vehicle- and P5091-treated CUTLL1 cells for the pulldown is shown. **K,** Immunoblots (WB) following immunoprecipitation (IP) of USP7 (left) and SRSF6 (right) in JURKAT cells, showing interaction of USP7 and SRSF6. **L,** Immunoblot studies for USP7 and SRSF6 using CUTLL1 and JURKAT cells upon treatment with increasing concentrations of P5091. Actin is used as a loading control. **M,** Immunoblot studies for USP7 and SRSF6 upon silencing of *USP7* using two different short-hairpin RNAs in CUTLL1 cells (left) or siRNA over a period of 96 hours in 293T cells (right). Actin is used as a loading control. **N,** Immunoblot analysis for SRSF6 levels upon treatment with cycloheximide (CHX; 200 μg/mL), or combination of cycloheximide with P5091 (10 μmol/L) over a period of 24 hours. Representative blot from one out of three experiments (left) and quantification of protein levels from three experiments (right) are shown (***, $P < 0.001$).

Published OnlineFirst May 22, 2020; DOI: 10.1158/2159-8290.CD-19-1436

led to an inhibition of T-ALL growth. Ectopic expression of SRSF6 rescued USP7 silencing-mediated inhibition of cell growth, confirming data from the P5091 study (Supplementary Fig. S9B and S9C).

We then silenced *SRSF6* (using the shRNA sh*SRSF6.0*) in the human T-ALL cell line CUTLL1 to show a significantly diminished growth of T-ALL cells (Fig. 3A). We further showed that even mild reduction of *SRSF6* levels (25%–40% silencing) using sh*SRSF6.1* and sh*SRSF6.2* significantly impairs T-ALL growth *in vitro* (Supplementary Fig. S9D and S9E) via an increase in apoptosis, accumulation of cells in the G_0–G_1 phase, and reduction of the actively proliferating cell population (Supplementary Fig. S10A and S10B). To assess the effect of SRSF6 silencing *in vivo* in human-to-mouse xenograft models, we transplanted CUTLL1 T-ALL cells expressing luciferase into immunocompromised mice. Assessment of cell growth using luminescence intensity and two different shRNAs for *SRSF6* at different time points showed that silencing of *SRSF6* leads to a delay in tumor growth (Fig. 3B; Supplementary Fig. S10C; left panel represents quantification of *in vivo* tumor growth over a period of 7 or 11 days; right panel depicts bioluminescence photos for representative mice per group are shown) and results in prolonged mouse survival (Fig. 3C). Gene expression patterns showed extensive changes upon SRSF6 silencing, presenting with 543 significantly upregulated genes and 1,001 downregulated genes (Fig. 3D). Of note, oncogenic targets of NOTCH1 [such as *NOTCH1* and *DELTEX1* (*DTX1*)] are among the downregulated transcripts (Fig. 3D; Supplementary Table S14). KEGG analysis of gene expression changes identified that spliceosome, proteasomal, cell cycle, and oncogenic transcripts are enriched (Fig. 3E). Changes in spliceosome-related transcript levels suggest that SRSF6 might regulate the levels of other splicing factors. This finding is in agreement with previous studies demonstrating that the activity of splicing factors, such as SRSF1, might control unproductive splicing via NMD of their own and other splicing-related transcripts (52). Similar to the previously documented role for SRSF proteins in regulating exon skipping, our splicing analysis demonstrated a marked reduction of skipped exons upon *SRSF6* silencing (Fig. 3F). We then interrogated the presence of overlapping alternatively spliced transcripts between USP7 inhibition and SRSF6 silencing that are also changed in T-ALL compared with T cells. We show that there was a significant overlap between transcripts alternatively spliced upon P5091 treatment as well as with transcripts alternatively spliced during the transition from $CD3^+$ T cells to T-ALL, with 342 transcripts commonly affected (Fig. 3G; Supplementary Fig. S10D). This analysis shows that SRSF6 mainly controls exon skipping in transcripts that are alternatively spliced in T-ALL compared with physiologic T cells.

Therapeutic Inhibition of Splicing in T-ALL

The aforementioned data also suggest that the splicing machinery is aberrantly regulated in T-ALL and inhibition of splicing activity could be a therapeutic avenue in T-ALL. Compounds that inhibit splicing in general and exon skipping in particular, such as the SRSF kinase protein inhibitors, have been studied extensively in blood cancers (2, 3, 79). Among them, the small-molecule inhibitor H3B-8800 is the most advanced in terms of translation to bedside, and has been used in clinical trials for acute myeloid leukemia, chronic myelomonocytic leukemia, and MDS (NCT02841540; ref. 80). H3B-8800 and its precursor drug E7107 both inhibit the U2 component SF3B1, and E7107 has been shown to be active against tumors with SRSF2 or SF3B1 mutations (3, 80). We hypothesize that T-ALL cells presenting abnormal splicing landscape might also be sensitive to H3B-8800 and that silencing of SRSF6 might further sensitize them to the drug.

To target the efficacy of splicing inhibition in our model, we treated T-ALL cell lines, including those with wild-type (CUTLL1) and mutant (JURKAT) SF3B1, with H3B-8800 (80, 81) for 72 hours. We included a second cell line with wild-type *SF3B1* (Cancer Cell Line Encyclopedia data, DND41 cells). T-ALL cell lines were sensitive to the inhibitor at concentrations similar to other cancer types with splicing mutations (80), with an IC_{50} value of about 30 nmol/L (Fig. 4A). This agrees with previous studies showing that the drug can block the activity of both wild-type and mutant SF3B1-containing spliceosomes (80). To further validate the effect of H3B-8800 in human T-ALL samples, we analyzed the growth of three diagnostic patient samples treated with H3B-8800 over a 3-day period, via counting live cells in the population. Similar to T-ALL cell lines, the three patient samples were sensitive to H3B-8800, and drug concentrations around 30 nmol/L resulted in significant (>50%) inhibition of cell growth in 3 days (Fig. 4B). We further confirmed these findings in a second group of three diagnostic samples expressing high levels of SRSF6 using the NADPH-based MTT assay upon treatment with vehicle or increasing concentrations of H3B-8800 over a period of 2 days (Supplementary Fig. S11A). In addition, treatment of mouse lineage-negative Sca/c-kit-positive (LSK) progenitor cells presented with lower lethality upon treatment with H3B-8800 in comparison with mouse T-ALL cells (ref. 41; Supplementary Fig. S11B and S11C), suggesting a significant therapeutic window. Analysis of the cell-cycle and apoptosis changes in both cell lines and patient samples showed a significant dose-dependent increase in apoptosis on day 2 of treatment (Fig. 4C; Supplementary Fig. S11D), and a reduction in the number of dividing cells (Supplementary Fig. S11E–S11G). Past studies have shown that cancers with splicing mutations exhibit increased sensitivity to splicing inhibitors, potentially due to the essentiality of splicing factors for survival (2, 3, 14). To test whether SRSF6 levels affect response to splicing inhibition, we treated control, sh*SRSF6.1*, and sh*SRSF6.2* cells with 30 nmol/L H3B-8800 over a period of 72 hours. We noticed that cells with lower levels of SRSF6 exhibit increased sensitivity to H3B-8800 treatment compared with control cells (Fig. 4D), in agreement with the effect of inhibitors in splicing factor–mutant cases. These findings suggest aberrant splicing can be a therapeutic vulnerability in T-ALL and a therapeutic implication of SRSF6 functionality in T-ALL.

Analysis of the splicing changes upon treatment of CUTLL1 and JURKAT cells with H3B-8800 over a period of 6 hours showed a significant enrichment in exon skipping and intron retention changes, similar to previous reports using H3B-8800 in solid tumors (ref. 80; Fig. 4E; Supplementary Fig. S12A). Splicing analysis upon a longer 24-hour treatment

Published OnlineFirst May 22, 2020; DOI: 10.1158/2159-8290.CD-19-1436

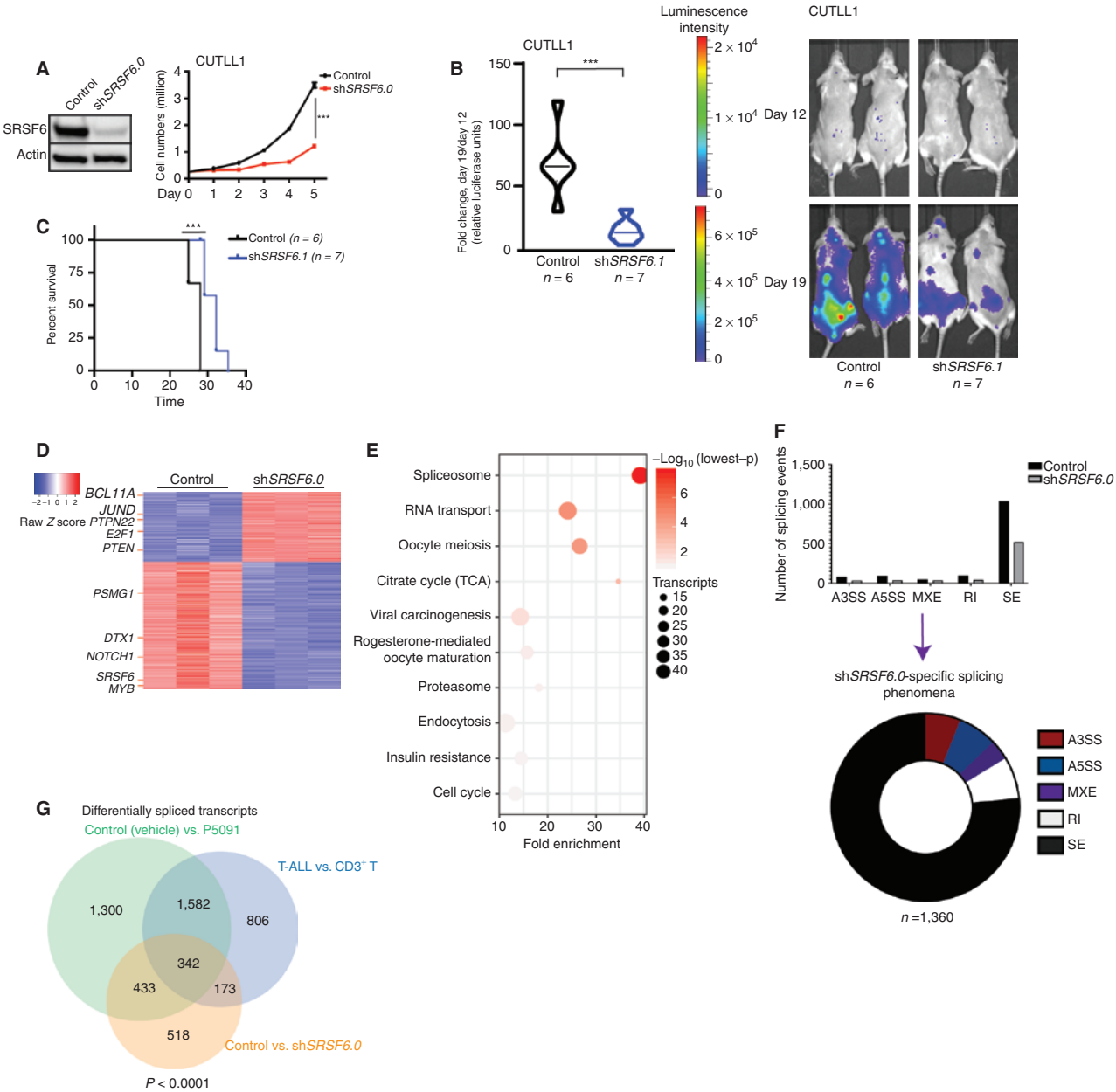

Figure 3. SRSF6 silencing inhibits T-ALL growth. **A,** Immunoblot analysis of SRSF6 protein levels (left) as well as growth of control- and sh*SRSF6*-expressing CUTLL1 cells over a period of 5 days ($n = 3$, right, ***, $P < 0.001$). Actin is used as loading control. **B,** Luciferase-expressing CUTLL1 cells were transduced with lentiviral vector expressing a control hairpin RNA or sh*SRSF6.1*, selected using puromycin for a period of 7 days, and injected intravenously into immunocompromised mice. Leukemic burden was assessed via blast detection in mouse body using bioluminescence and IVIS equipment twice per week. Relative bioluminescence intensity is shown for two representative mice per treatment group on days 12 and 19 of treatment (right). The fold change in total flux from day 12 to day 19 is shown on the left (control, $n = 6$; sh*SRSF6.1*, $n = 7$, ***, $P < 0.001$). **C,** Survival analysis of mice transplanted with control hairpin RNA or sh*SRSF6.1*-expressing CUTLL1 cells (control, $n = 6$; sh*SRSF6.1*, $n = 7$, ***, $P < 0.001$). **D,** Heat map of changes in gene expression representing 543 significantly upregulated genes and 1,001 downregulated genes in sh*SRSF6.0*-expressing compared with control JURKAT cells (adj. $P < 0.01$). **E,** KEGG analysis showing main transcript pathways enriched for gene expression changes in sh*SRSF6.0*-expressing JURKAT cells compared with the control JURKAT population. **F,** Splicing analysis in the sh*SRSF6.0* sample and comparison with control JURKAT cells. Bar graph (top) represents different types of splicing events in each genotype; pie chart (bottom) shows sh*SRSF6.0*-specific splicing phenomena. Skipped exons (SE) is the main event category. The plot represents the MATS analysis using three biological replicates per group. Only events that passed the statistics threshold (FDR < 0.05) and present with PSI > 0.1 are presented. **G,** Overlap of transcripts presenting with splicing changes in DMSO (vehicle) versus P5091, $CD3^+$ T cells versus T-ALL cells, as well as control versus sh*SRSF6.0* conditions. Analysis shows 342 genes common in all comparisons ($P < 0.0001$).

Published OnlineFirst May 22, 2020; DOI: 10.1158/2159-8290.CD-19-1436

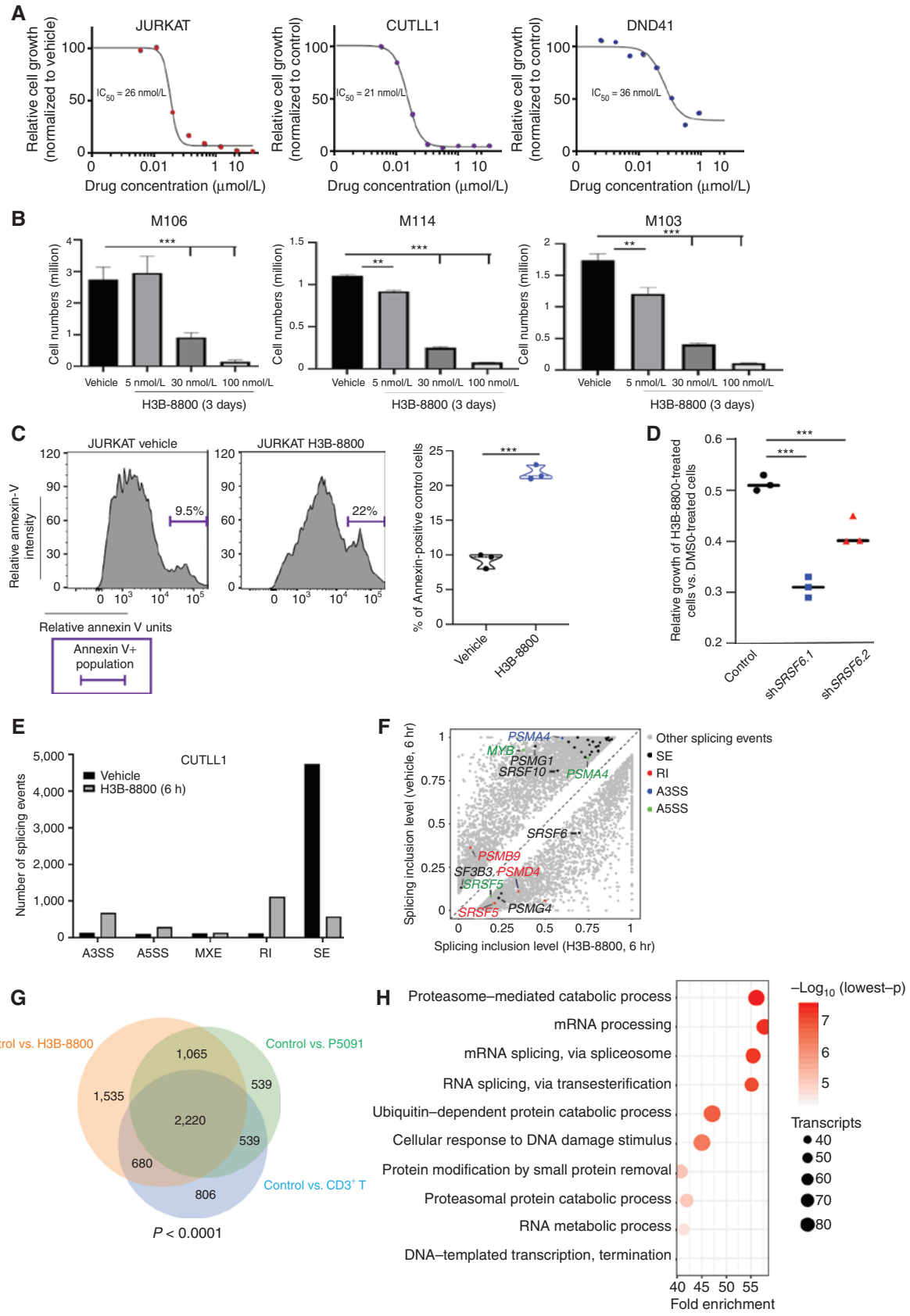

Published OnlineFirst May 22, 2020; DOI: 10.1158/2159-8290.CD-19-1436

of JURKAT cells with H3B-8800 led to conclusions similar to the 6-hour treatment (Supplementary Fig. S12B and S12C). More specifically, proteasomal subunits, such as *PSMB9* and *PSMD4*, are altered whereas the transcript of the proteasome chaperone *PSMG1* (82–84) is the proteasome-related transcript whose splicing is the most significantly altered in H3B-8800–treated cells (Fig. 4F; Supplementary Fig. S12D). We also sequenced the same libraries for JURKAT cells treated with control (DMSO) or H3B-8800, at 300PE (150/150) using Illumina technology. This showed there are no differences in the splicing changes identified upon use of longer sequencing reads (Supplementary Fig. S12E–S12G). As the rMATS algorithm we use in our analyses performs better with longer reads, we also employed two additional methods to confirm splicing changes: we used Cufflinks and Cuffdiff for isoform prediction and differential expression analysis of those isoforms (85), a read length–dependent method, as well as the exon usage method DEXSeq that predicts differential exon usage and is read length–independent (86). In DEXSeq, only the exon coverages are compared regardless of which isoform they belong to. Data analysis showed a significant overlap between transcripts with differentially spliced events from the rMATS analysis, differential isoform expression from the Cuffdiff analysis, and transcripts with differentially used exons from the DEXSeq analysis, further underlining the validity of our conclusions drawn from the use of rMATS analysis and suggesting that the most prevalent splicing change between the control (DMSO) and H3B-8800–treated JURKAT cells was exon-related (Supplementary Fig. S12H). The overlapping transcript group is enriched in cell-cycle and proteasomal transcripts (Supplementary Fig. S12I). In addition, we noticed that splicing inhibition affects SRSF6 splicing, leading to a reduced SRSF6 transcript and protein expression (Fig. 4F; Supplementary Fig. S12J and S12K), further underscoring the interdependency among splicing factors. As USP7 controls the stability of SRSF proteins, we sought to study the effect of USP7 inhibition on the splicing landscape in T-ALL cells. In agreement with our previous findings on the impact of USP7 on SRSF biology, we identified a significant change in exon skipping phenomena upon treatment with P5091 USP7 inhibitor (Supplementary Fig. S13A and S13B). Our studies also show a significant overlap in transcripts affected by splicing in the transition from $CD3^+$ T cells to T-ALL as well as between H3B-8800– or P5091-treated T-ALL cells and vehicle-treated cells (Fig. 4G; Supplementary Fig. S13C–S13E). These findings suggest that splicing or USP7 inhibition affect the splicing of critical transcripts that are aberrantly spliced in T-ALL compared with T cells. Gene ontology analysis of the overlapping alternative spliced transcripts (Fig. 4G) showed an enrichment for spliceosome, DNA damage response, and proteasomal transcripts (Fig. 4H).

Aberrant Splicing of Proteasomal Subunits Can Be Exploited for Therapeutic Purposes in T-ALL

As mentioned above, *PSMG1* is the top alternatively spliced proteasome-related transcript upon H3B-8800 treatment. Further analysis showed that there is an exon 4 skipping event in about 50% (or PSI = 0.5) of the PSMG1 transcripts, leading to a switch between two *PSMG1* transcripts in both CUTLL1 and JURKAT cells upon treatment with H3B-8800 (CCDS13660 and CCDS13661; Fig. 5A; Supplementary Fig. S13F). Our gene expression analysis showed a significant decrease in PSMG1 transcript levels upon treatment with H3B-8800 (see values in *y*-axis representing exon expression levels, Fig. 5A). Targeted PCR analysis using primers flanking *PSMG1* exon 4 confirmed exon 4 skipping upon splicing inhibition via H3B-8800 treatment (Fig. 5B and C). As USP7 controls exon skipping in T-ALL (Supplementary Fig. S13A and S13B), we studied alterations in *PSMG1* splicing in our data from USP7 inhibition on the splicing landscape in T-ALL cells. In agreement with our previous findings using H3B-8800, P5091 treatment led to a similar, albeit significantly weaker compared with H3B-8800 treatment, exon 4 skipping phenotype in *PSMG1* affecting 11% of the transcripts (PSI = 0.11, Fig. 5D; Supplementary Fig. S13G).

Skipping of exon 4 leads to a 21 amino acid deletion (131–152; Supplementary Fig. S14A) yielding the shorter PSMG1-202 isoform. Structure modeling showed that 202 presents with a significant protein structure alteration (Fig. 5E; Supplementary Fig. S14B). As PSMG1 forms a heterodimer with PSMG2 to serve as a chaperone for the core proteasome alpha ring subunits 5 and 7 (PSMA5 and PSMA7; refs. 82, 84) critical for proteasome formation, disruption of PSMG1 levels might alter proteasomal function. PSMG1-depleted cells present with incomplete proteasomes and presumably reduced proteasome activities (82, 84). Indeed, our assay for

Figure 4. Inhibition of splicing blocks the growth of T-cell leukemia tumors. **A,** IC_{50} curves of splicing inhibition using H3B-8800 in T-ALL cell lines (JURKAT, CUTLL1, DND41) over a period of 72 hours. To study cell growth, 3,000 cells per well were used and incubated with AlamarBlue for 4 hours. **B,** Cell numbers for three patient samples treated with vehicle and increasing concentrations of H3B-8800 up to 100 nmol/L over a 72-hour period. Live human T-cell leukemia cell populations were measured using cytometry and staining with hCD7 and hCD45 antibodies (***, $P < 0.001$). **C,** Annexin V staining plots (left) and quantification (right) upon treatment with 30 nmol/L H3B-8800 over a period of 48 hours in JURKAT T-ALL cells ($n = 3$, ***, $P < 0.001$). **D,** Relative growth of H3B-8800–treated cells compared with vehicle-treated cells is shown for *control*, sh*SRSF6.1*, and sh*SRSF6.2*-expressing CUTLL1 cell populations. sh*SRSF6.1*-expressing cells present with an increased sensitivity to splicing inhibition compared with control cells ($n = 3$, ***, $P < 0.001$). **E,** Number of splicing events in CUTLL1 cells upon treatment with H3B-8800 for 6 hours versus DMSO (vehicle). Retained introns (RI) and skipped exons (SE) were the two event categories affected most dramatically. The plot represents the MATS analysis using three biological replicates per group. Only events that passed the statistics threshold (FDR < 0.05) and PSI > 0.1 are presented. **F,** Scatter plot of splicing changes and distribution in H3B-8800–treated CUTLL1 cells (6 hours) compared with vehicle-treated CUTLL1 cells. Selected transcripts are colored by the type of differentially spliced event. Splicing is quantified using a "percent spliced in" value (PSI, or ψ value) and changes affecting at least 10% of transcripts are presented. **G,** Overlapping of transcripts affected by splicing changes in vehicle-treated JURKAT cells in comparison with H3B-8800- and P5091-treated JURKAT cells as well as $CD3^+$ T cells. Analysis identified 2,220 transcripts alternatively spliced in vehicle-treated JURKAT cells compared with the three other conditions. **H,** Gene ontology analysis of 2,220 overlapping genes from **G,** showing enrichment of critical transcript families, including the proteasome and spliceosome machinery-encoding transcripts.

Published OnlineFirst May 22, 2020; DOI: 10.1158/2159-8290.CD-19-1436

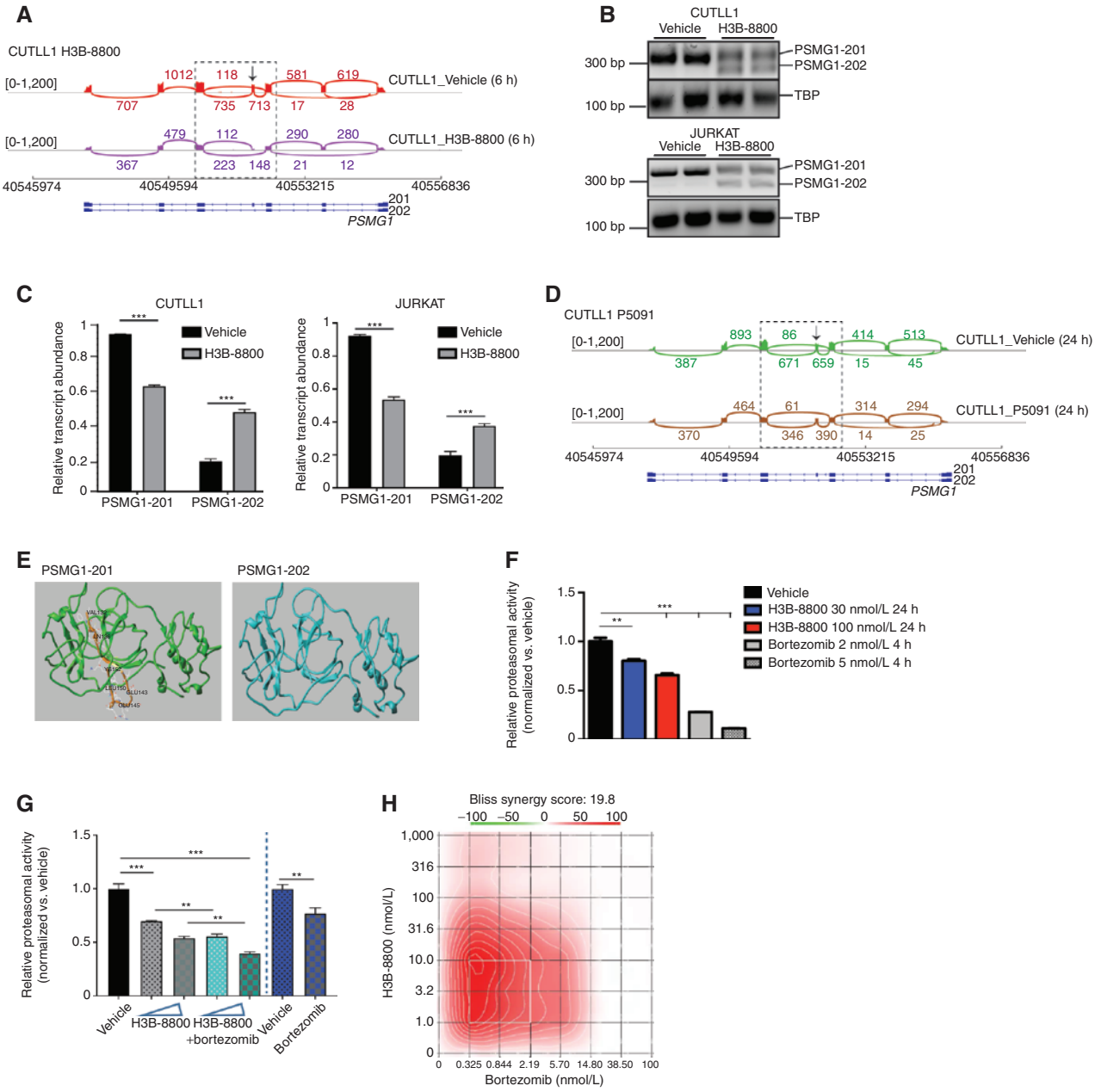

Figure 5. Extensive splicing changes affecting proteasome subunits is a vulnerability in T-cell leukemia. **A,** Sashimi plots representing splicing and exon–exon junctions for the *PSMG1* transcript in CUTLL1 cells treated with 30 nmol/L H3B-8800 for 6 hours. DNA/gene is shown along the horizontal axis. Thicker sections represent exons coding for protein sequence. Numbers over the lines connecting exons represent the number of reads mapped to that exon–exon junction. **B,** PCR-based analysis coupled to electrophoresis for detection of PSMG1-201 and PSMG-202 isoforms upon H3B-8800 treatment (30 nmol/L, 6 hours) using CUTLL1 (top) and JURKAT (bottom) cells. **C,** Quantification of band intensities presented in **B**. ***, $P \leq 0.001$. **D,** Sashimi plots representing splicing and exon–exon junctions for the *PSMG1* transcript in CUTLL1 cells treated with 10 μmol/L P5091 for 24 hours. DNA/gene is shown along the horizontal axis. Thicker sections represent exons coding for protein sequence. Numbers over the lines connecting exons represent the number of reads mapped to that junction. **E,** Modeling of PSMG1 protein structure changes upon H3B-8800 treatment. Structures of constructs 201 and 202 [consensus coding sequence (CCDS) CCDS13660 and CCDS13661 correspondingly for protein Q95456] were displayed. Brown and yellow part represents 21 amino acids present in 201 but missing from 202. Amino acids VAL123, GLN136, GLU143, GLN145, LEU150, and CYS152 are highlighted. **F,** Measurement of proteasome activity using a luminescence-based method upon treatment of JURKAT cells with 30 nmol/L and 100 nmol/L H3B-8800 for 24 hours. Bortezomib was used as a positive control for proteasome inhibition (**, $P < 0.01$; ***, $P < 0.001$). **G,** Measurement of proteasome activity using a luminescence-based method upon treatment of JURKAT cells with 30 nmol/L and 100 nmol/L H3B-8800 for 24 hours, alone (gray bars) or in combination with 0.5 nmol/L bortezomib (4-hour treatment, green bars). Bortezomib was used as a positive control for proteasome inhibition (0.5 nmol/L, 4-hour treatment, blue bar, **, $P < 0.01$; ***, $P < 0.001$). **H,** Synergy heat maps for proteasomal inhibitor bortezomib and H3B-8800 treatment over a period of 3 days in JURKAT cells. Bliss analysis is shown. This result indicates synergy at the lower dose range for both drugs that might allow for combinatorial drug treatment with minimum toxicity.

proteasomal activity shows that splicing inhibition significantly impairs proteasomal activity in a drug dose–dependent manner (Fig. 5F). Aberrant proteasomal regulation has been implicated in cancer and hematologic malignancies in particular, such as in leukemia as well as multiple myeloma (77, 87, 88). Higher levels of PSMG1 in T-ALL compared with T cells also suggest a higher proteasomal activity in this disease (Supplementary Fig. S14C). Inhibition of proteasomal function is the frontline therapy in multiple myeloma and it has also been suggested as a therapeutic strategy in preclinical testing in T-ALL and B-cell ALL, mainly via its implications for the regulation of NOTCH1 targets as well as the NFκB pathway (87). Moreover, USP7 inhibition has been proposed to lead to sensitivity against proteasomal inhibitors in multiple myeloma (77).

On the basis of the aforementioned findings, we hypothesized that splicing inhibition can perturb aberrant proteasome function in T-ALL and could act synergistically to proteasome inhibition. To test this hypothesis, we initially showed that the T-ALL lines CUTLL1 and JURKAT are sensitive at the nanomolar range of concentrations to the clinically used proteasomal inhibitor bortezomib (Supplementary Fig. S14D). We then asked whether the combination of splicing (H3B-8800) and proteasome (bortezomib or carfilzomib) inhibition could act synergistically in blocking disease growth. We used a range of concentrations for H3B-8800 and carfilzomib or bortezomib in the range of previously used doses in blood and solid tumors (87, 89, 90). We noticed an enhanced activity of combinations of H3B-8800 and bortezomib as well as P5091 and bortezomib in suppressing proteasome activity (Fig. 5G; Supplementary Fig. S14E) and a strong synergistic effect against T-ALL cell growth *in vitro* (*Bliss* analysis, ref. 91; Fig. 5H; Supplementary Fig. S14F). Use of a carfilzomib and H3B-8800 combination led to similar conclusions (Supplementary Fig. S14G).

To test the therapeutic window of the combinatorial treatment, we treated human CD34$^+$ hematopoietic progenitor cells from the cord blood with H3B-8000, bortezomib, and their combination. Initially, we noticed that CD34$^+$ cells are less sensitive than T-ALL patient samples and cell lines at the 30 nmol/L H3B-8800 concentration (Supplementary Fig. S15A and comparison to Fig. 4A and B). Although CD34$^+$ cells are sensitive to bortezomib treatment at concentrations similar to T-ALL samples (Supplementary Fig. S15B), treatment of CD34$^+$ with doses of bortezomib and H3B-8800 that synergistically led to a significant inhibition of T-ALL growth (see heat map in Fig. 5H) led to a very mild effect on CD34$^+$ growth (Supplementary Fig. S15C and S15D).

To assess a potential role for the PSMG1 exon 4 skipping in therapy resistance, we designed antisense oligos (ASO) with the aim to block exon skipping and thus block an increase of the 202 isoform of *PSMG1* upon application of H3B-8800 onto T-ALL cells. By using different combinations of two different ASOs, we managed to partially block exon 4 skipping of *PSMG1* (~25% reduction in 202 allele, Supplementary Fig. S15E–S15G). Treatment with bortezomib as well as the splicing inhibitor H3B-8800 both presented with a decreased sensitivity of the ASO-expressing cells toward therapy, suggesting that further modulation of *PSMG1* splicing might pave the way for therapeutic intervention in acute leukemia (Supplementary Fig. S15H and S15I).

DISCUSSION

In this study, we characterized splicing changes and associated molecular underpinnings in T-ALL. Our findings suggest that USP7 controls the posttranslational levels of SRSF6 factors in T-ALL leading to aberrant splicing regulation (Fig. 6). Our study reinforces findings in recent studies in blood and other malignancies that there is extensive aberrant splicing in cancer in the absence or presence of mutations affecting the splicing machinery (5, 13, 92, 93). We show that the transcripts affected by abnormal splicing include cell cycle–related proteins, epigenetic modifiers, and proteasomal subunits, all of which represent therapeutic vulnerabilities in this disease.

Our study compares a differentiated total T-cell population (CD3$^+$) or the CD4$^+$ T cell subset from the peripheral blood to undifferentiated thymocytes. We show that CD3$^+$ and CD4$^+$ T cells present with similarities in the splicing landscape and splicing phenomena distinct from thymocytes, with an extensive number of cell cycle–related transcript differentials between thymocytes and differentiated CD3$^+$/CD4$^+$ T cells. Thus, splicing might reflect the developmental stage of T cells. In addition, T cells were significantly different from T-ALL patient cells with regard to the splicing landscape, and disease cases with HR for relapse exhibited a significant number of mutually exclusive exons and skipped exon phenomena different from the NHR cases, suggesting that splicing might be a good indicator of disease status.

Proteasome, cell cycle, and epigenetic enzymes are critical gene ontology terms significantly altered between T cells and the different disease subtypes. In this study, we identified components of the 20S and 19S proteasome as well as the proteasome chaperone PSMG1 that are differentially spliced in T-ALL compared with T cells. *In silico* modeling of PSMG1 structure showed extensive changes in protein structure in T-ALL, and our experiments demonstrate that inhibition of the splicing machinery affects proteasomal function. We further show that the components of the splicing machinery might be regulated at the posttranslational level via the activity of deubiquitinases and we present regulation of SRSF6 by USP7 as a proof-of-principle. Hitherto, efforts toward understanding splicing factor regulation in cancer at the nongenetic level have mainly focused on transcriptional control via oncogenic factors such as MYC (18, 67). In addition, our findings suggest that SRSF6 might be regulated via NMD in T cells but not in T-ALL, as we noticed a significant reduction of the NMD-related allele in T-ALL and its reappearance upon silencing of the UPF1 component of the NMD machinery (refs. 51, 52; Supplementary Fig. S3C–S3G). Further investigation is required to properly address the role of the NMD process upon SRSF levels in T-ALL as well as potential feedforward loops between transcriptional regulation, NMD, and posttranslational regulation.

Although posttranslational modifications, such as methylation via arginine methyltransferases and phosphorylation via SRSF protein kinases in particular, have been previously suggested as a means of regulating splicing factor activity

Published OnlineFirst May 22, 2020; DOI: 10.1158/2159-8290.CD-19-1436

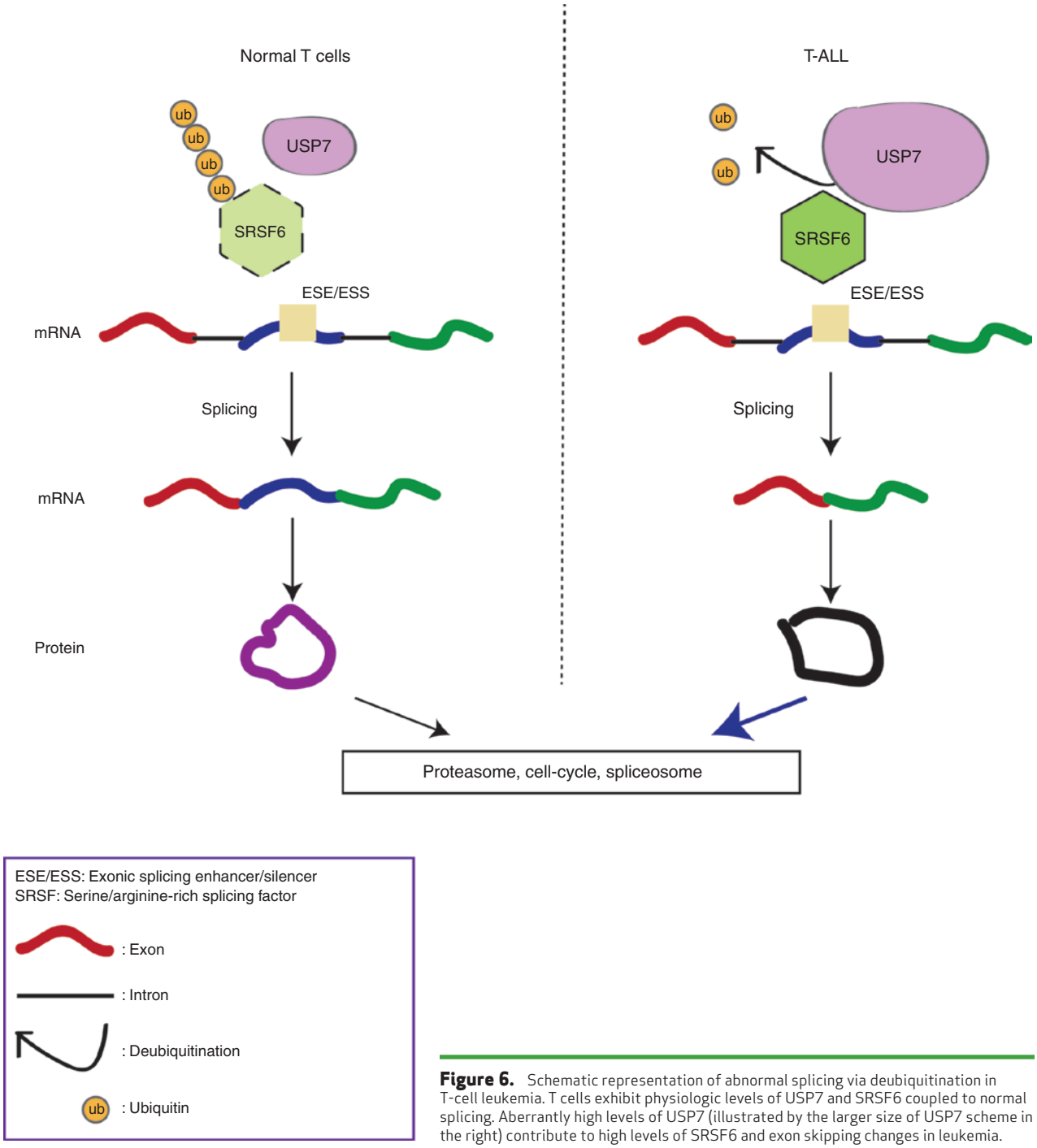

Figure 6. Schematic representation of abnormal splicing via deubiquitination in T-cell leukemia. T cells exhibit physiologic levels of USP7 and SRSF6 coupled to normal splicing. Aberrantly high levels of USP7 (illustrated by the larger size of USP7 scheme in the right) contribute to high levels of SRSF6 and exon skipping changes in leukemia.

(66, 79, 94–98), there is very little information on how ubiquitination or similar modifications controls splicing factor levels or activity (71, 72, 99–103), especially in cancer systems. Further investigation is warranted to identify and characterize different types of splicing factor ubiquitination and whether it mediates effects other than regulation of the protein levels. We further show that modulation of USP7 activity or SRSF6 levels leads to changes in the expression and/or splicing pattern of the transcripts of other splicing factors. This suggests that SRSF6 regulates the levels of other splicing transcripts. Indeed, it has been reported in the past that a few initial changes in the activity or levels of splicing factors can subsequently lead to extensive changes to the splicing landscape of spliceosome transcripts via controlling unproductive splicing leading to NMD (52). Spliceosome-related transcript changes with regard to splicing and expression between cancer and physiology as well as upon splicing inhibition might be similarly explained via alterations in the levels or SRSF6 or SF3B1 (in the case of H3B-8800). These findings warrant further investigation in cancer.

Published OnlineFirst May 22, 2020; DOI: 10.1158/2159-8290.CD-19-1436

In the realm of blood cancers, clinical trials have been evaluating the potential of splicing-targeted compounds in myeloid malignancies and premalignant lesions. Similar therapeutic approaches might be employed in T-ALL, a disease without splicing factor mutations. We show that treatment with splicing or deubiquitinase inhibitors affects splicing in disease-related transcripts and blocks T-ALL growth. Our study extends the findings of previous studies suggesting that targeting protein levels of SF3B1 via blocking deubiquitination could be exploited in cancers with *SF3B1* mutations (104). We demonstrate that deubiquitination actively controls splicing factor stability, and inhibition of deubiquitination can be a valid therapeutic strategy in cancer in the presence or absence of splicing mutations. To assess whether splicing inhibition could act in a combinatorial fashion with other drugs currently in use in preclinical or clinical practice, we used combinations of proteasomal and splicing inhibitors as well as deubiquitinase and splicing inhibitors to demonstrate a synergistic effect in inhibiting leukemia growth. Similar to previously suggested alternative methods of targeting the splicing machinery, including arginine methyltransferase inhibitors (96, 97), our study elucidated a method of targeting splicing via inhibition of deubiquitination and paves the way for further testing this therapeutic modality in additional cancer types with or without splicing factor mutations. Our studies also suggest a potential therapeutic window upon combinatorial drug treatment, as H3B-8800 and combination with proteasome inhibition are not similarly efficient in inhibiting normal mouse and human hematopoietic progenitor growth *in vitro*. This conclusion is in agreement with recent clinical data using H3B-8800, which suggest that the drug might be safe even after prolonged dosing (105). Additional preclinical studies are warranted to evaluate the toxicity and efficacy for the use of combinations of splicing and proteasomal inhibitors.

Whether SRSF proteins functionally and physically interact with oncogenes or pro-oncogenic cofactors to regulate splicing or other RNA-related processes, including transcriptional elongation, is hitherto relatively undercharacterized. A recent study showed that BRD4 might coordinate splicing and transcriptional elongation via interaction with the splicing machinery (50). SRSF proteins, including SRSF6, have not been identified as NOTCH1 interactants in published NOTCH1 mass spectrometry studies (106, 107), and our studies show that NOTCH1 inhibition does not affect SRSF6 levels. Nevertheless, the role of NOTCH1, and potentially other oncogenes, in the transcriptional and posttranslational regulation of SRSF proteins nonetheless warrants further investigation.

In conclusion, our study provides new proof-of-principle for posttranslational regulation of SRSFs, independent of splicing factor mutations, and suggests new combinatorial treatment in leukemia, a concept that might apply to additional tumors in the presence or absence of splicing mutations.

METHODS

Cell Lines and Primary Cells

The human T-ALL cell lines CUTLL1 (gift from Adolfo Ferrando, Columbia University, New York, NY), JURKAT (ATCC, #CCL-119), and DND41 (ATCC) were cultured in RPMI1640 medium supplemented with 10% heat-inactivated FBS (Sigma-Aldrich), 2% penicillin/streptomycin (Gibco, Thermo Fisher Scientific), and 1% GlutaMAX (Gibco, Thermo Fisher Scientific). 293T cells (ATCC, #CRL-11268) were maintained in DMEM supplemented with 10% heat-inactivated FBS, 2% penicillin/streptomycin, and 1% GlutaMAX. The cells were periodically tested for the presence of *Mycoplasma* using the Lonza Walkersville MycoAlert Mycoplasma Detection Kit (last test in January 2020). The cell lines were kept in culture for a maximum of 20 passages and were authenticated using short-tandem repeat profiling (JURKAT and DND41) or using PCR to detect the TCRb-NOTCH1 translocation in CUTLL1 cells (*TCRBJ2S4F:5′*-GGACCCGGCTCTCAGTGCT-3′, *NOTCH1R:5′*-TCCCGCCCTCCAAAATAAGG-3′). Last cell authentication was performed in February 2020. Human $CD3^+$, $CD8^+$, and $CD4^+$ T cells were purchased from AllCells.com or from Astarte Biologics. Primary human samples were collected by collaborating institutions with written informed consent and analyzed under the supervision of the Institutional Review Board of Padova University, the Associazone Italiana Ematologia Oncologia Pediatrica, and the Berlin-Frankfurt-Münster (AIEOP-BFM) ALL 2000/2006 pediatric clinical trials. Written informed consent for the use of leftover material for research purposes was obtained from all of the patients at trial entry in accordance with the Declaration of Helsinki.

Antibodies and Reagents

The following antibodies were used for Western blotting or immuneprecipitation: mouse anti-actin (Millipore, clone C4), rabbit anti-SRSF6 [Bethyl Laboratories, A303-669A, and Abcam (ab140602)], rabbit anti-SRSF3 (Abcam, ab73891), rabbit anti-SF3B1 [MLB (D221-3)], rabbit anti-USP7 [Bethyl Laboratories (A300-033A-7)], rabbit anti-cleaved NOTCH1 [Val1744; Cell Signaling Technology (4147)], and rabbit anti-Lamin B1 [ProteinTech Group (12987-1-AP)]. HA antibody (C29F4, catalog no. 3724) was purchased from Cell Signaling Technology. Secondary antibodies for Western blots were horseradish peroxidase–conjugated anti-rabbit and anti-mouse IgG (GE Healthcare). Quick Start Bovine Gamma Globulin (BGG) Standard Set protein standards were purchased from Bio-Rad. Benzonase nuclease, RNase A, and dithiothreitol (DTT) were purchased from Sigma-Aldrich. NaV and NaF were purchased from New England BioLabs. Protein G Dynabeads were purchased from Life Technologies. IgG-free BSA was purchased from Jackson ImmunoResearch Laboratories. Phenol chloroform was purchased from Thermo Fisher Scientific. Proteinase K, Tousimis formaldehyde, and MG132 reagent were purchased from Thermo Fisher Scientific. USP7 inhibitor P5091 was purchased from Selleckchem. H3B-8800 was obtained through collaboration with H3 Biomedicine.

Gel Filtration and Immunoprecipitation

Gel filtration was performed using whole-cell extracts and a Superose 6 column to separate complexes from 5 MDa to 5 KDa. Immunoprecipitation and mass spectrometry studies were performed as described previously (69): 200 million cells were incubated in TENT buffer [50 mmol/L Tris pH 7.5, 5 mmol/L EDTA, 150 mmol/L NaCl, 0.05% v/v Tween 20, 1:100 protease inhibitor (Sigma-Aldrich, P8340), 1 mmol/L NaV, 1 mmol/L NaF, and 0.5 mmol/L DTT in H_2O] supplemented with 5 mmol/L $MgCl_2$ and 100 units benzonase, and incubated at 4°C for 30 minutes, with rotation. Lysates were passed through a $25^{1/2}$G needle/syringe three times and spun down at 4°C, 2,000 rpm, for 7 minutes to remove debris. Lysates were then incubated with the appropriate antibody-conjugated beads (15 μg antibody) at 4°C overnight, with rotation. Beads were washed four times in TENT buffer at 4°C for 3 minutes, and protein complexes were eluted in 50 μL 0.1 mol/L glycine, pH 2.5, for 10 minutes at 25°C, with shaking, followed by addition of 5 μL of 1 mol/L Tris pH 8.0 to the supernatants.

Published OnlineFirst May 22, 2020; DOI: 10.1158/2159-8290.CD-19-1436

Sample Preparation for Mass Spectrometry

Immunoprecipitated proteins were processed for acetone precipitation and the purified protein pellet was denatured in 50 μL of 8 mol/L urea/0.4 mol/L ammonium bicarbonate followed by reduction in 2 μL of 100 mmol/L DTT. Protein was alkylated with 18 mmol/L iodoacetamide for 30 minutes at room temperature in the dark. Samples were diluted with four volumes of water to bring urea concentration to 1.8 mol/L. Sequencing-grade trypsin (Promega) was added at 1:50 (enzyme:substrate) and incubated at 37°C overnight. The digests were acidified to 0.5% trifluoroacetic acid (TFA) and the peptides were desalted on C18 Sep-Paks (Waters). Peptides were eluted with 2 × 50 μL of 80% acetonitrile (ACN)/0.1% TFA to ensure complete recovery. The pooled extracts were dried in a vacuum concentrator and resuspended in 30 μL of 5% ACN/0.1% formic acid (FA) for LC/MS analysis.

For the ubiquitin analysis, PTMScan Ubiquitin Remnant Motif (K–GG) Kit was used following manufacturer's instructions (Cell Signaling Technology, Inc).

LC/MS-MS Analysis

Peptides were analyzed by LC/MS-MS using a Dionex UltiMate 3000 Rapid Separation nanoLC and either an Orbitrap Velos Mass Spectrometer or QEHF (Thermo Fisher Scientific Inc). Samples were loaded onto the trap column, which was 150 μm × 3 cm in-house packed with 3 um ReproSil-Pur beads. The analytic column was a 75 μm × 10.5 cm PicoChip column packed with 3 μm ReproSil-Pur beads (New Objective, Inc.). The flow rate was kept at 300 nL/minute. Solvent A was 0.1% FA in water and Solvent B was 0.1% FA in ACN. The peptide was separated on a 120-minute analytic gradient from 5% ACN/0.1% FA to 40% ACN/0.1% FA. Previously selected ions were dynamically excluded from reselection for 60 seconds. Proteins were identified from the MS raw files using the Mascot search engine (Matrix Science, version 2.5.1). MS-MS spectra were searched against the SwissProt human database. All searches included carbamidomethyl cysteine as a fixed modification and oxidized MET, deamidated ASN and GLN, and acetylated N-term as variable modifications. Diglycine on Lys was set as a variable modification for ubiquitin detection. Three missed tryptic cleavages were allowed. A 1% FDR cutoff was applied at the peptide level. Only proteins with a minimum of two peptides above the cutoff were considered for further study. Identified peptides/protein were visualized by Scaffold software (version 4.9.0, Proteome Software Inc.).

Immunoblots and RPPA

Up to 10 million cells were collected to prepare whole-cell extracts, as described previously (69), and resuspended in 40 μL RIPA buffer (50 mmol/L Tris HCl pH 8.0, 150 mmol/L NaCl, 1% NP-40/IGEPAL, 0.5% sodium deoxycholate, 0.1% SDS, 1:100 protease inhibitor (Sigma-Aldrich, P8340), 1 mmol/L NaV, and 1 mmol/L NaF in H_2O) per 2 million cells. RPPA was performed as described previously (69, 108, 109). Briefly, cells were lysed in an appropriate lysis buffer with protease and phosphatase inhibitors, serially diluted into four-point dilution curves, and printed on nitrocellulose-coated glass slides using the Aushon 2470 Arrayer (Aushon Biosystems).

CRISPR/Cas9 Screen

A previously described sgRNA domain-focused approach was used in the screen, which enhances CRISPR/Cas9-negative selection by targeting a functional protein domain. Individual sgRNAs were subcloned into a lentivirus-based GFP-tagged sgRNA vector and transfected into different types of tumor cell lines for a loss-of-function pooled screen. Genomic DNA was harvested from cells on day 4 and day 20 posttransduction of sgRNA library, and individual sgRNA read counts were evaluated by next-generation sequencing. Changes in sgRNA abundance were assessed by measuring the average fold change (day4/day20) of all sgRNAs targeting a given gene.

Targeted Sequencing

The library was captured with Nimblegen SeqCap and sequenced using Illumina technology. The alignment was done by Burrows-Wheeler Aligner (BWA) and the variants called by genome analysis toolkit (GATK) and annotated using the single-nucleotide polymorphism database (dbSNP) and SnpEff. The variant was filtered for impact (high or moderate) and checked for missense mutations in the coding sequence of our genes using Integrative Genomics Viewer (IGV).

RNA Isolation, Sequencing, and PCR

RNA was extracted from cell lines and patient samples using Bio-Rad total RNA isolation kit. Poly(A)-selected, unstranded Illumina libraries were generated using the TruSeq RNA kit from Illumina. Library fragments were amplified with PCR (15 cycles), size-selected using AMPure XP beads to select for fragments between 200 and 500 bp, and sequenced on the Illumina NextSeq 500 in a paired-end run (2 × 76-bp) for a sequencing depth of about 80 million reads per sample.

Primers:

PSMG1-F: TGGGAGGAAGTTGGTTGTGC
PSMG1-R: GGACAACACGCCGAGTCTTT
SRSF2-exon2-F: CTATGGATGCCATGGACGGG
SRSF2-exon2-R: CTCCGTTTACACTGCTTGCC
SRSF6-exon3-F: GACGGCTACAGCTACGGAAG
SRSF6-exon3-R: GCCAACTGCACCGACTAGAA
SRSF7-cryptic-F: TGCAGAAGATGCAGTACGAGG
SRSF7-cryptic-R: AGCGAGAGTATCGCCTTCCT

Real-time primers:

SRSF6-NMD-F CTTTGGCTGACCTTACCGGA
SRSF6-NMD-R TCCGACTGCTGTATCCACCT

ASOs designed to block exon skipping in *PSMG1*:

ASO1: 0120_1739_2OM_E4 5′ - mC*mC*mU*mG*mG*mC*mU*mC*mC*mA*mC*mU*mA*mU*mU*mG*mA*mC*mC*mU*mA*mC - 3′

ASO2: 0120_1740_2OM_E4 5′ - mA*mA*mG*mU*mU*mC*mC*mA*mC*mG*mC*mU*mU*mU*mU*mU*mG*mU*mC*mA*mA*mG*mU*mA*mA*mG*mU*mU*mU*mU*mA*mU*mA*mC*mA*mC*mC*mA - 3′

The positive control ASO is designed to promote exon skipping of *C1orf43* gene:

CAU CCA GAG CUU UCA UCC UAU ACA GAU AGU UG.

The following information was taken into consideration upon designing the ASO: (i) every base is 2′ O-Methyl RNA, (ii) every base is linked by phosphorothioate bond, (iii) we performed a 100 nmol/L synthesis scale coupled to HPLC purification. ASO transfection was performed using 100 nmol/L or 200 nmol/L final concentration of each ASO based on the Lipofectamine 3000 Transfection reagent from Thermo Scientific following manufacturer's guidelines. In brief, 6 μL of P3000 and 6 μL of lipofectamine for each condition to transfect 800,000 T-ALL cells per well of a 6-well plate.

Bioinformatics Analysis

RNA-sequencing reads were mapped to human genome hg19 using TopHat. Differential gene expression analysis was performed using the EdgeR package in R. Gene expression changes were visualized in heat maps using the ggplot2 package in R. rMATS version 4.0.2 was used to perform alternative splicing analysis with human Ensembl.GRCh37v75 as the annotation. The exon count tables and differential exon usage was calculated using DEXSeq (v3.10; ref. 86). Isoform predictions and isoform differential expression analysis were analyzed using Cufflinks and Cuffdiff (v 2.2.1; PMID:

Published OnlineFirst May 22, 2020; DOI: 10.1158/2159-8290.CD-19-1436

20436464; ref. 85). In all related figures, rMATS bargraphs present events that passed the statistical threshold (FDR controlled *P* value <0.05 and PSI > 0.1). To compare the level of similarity among the samples and their replicates, we used two methods: principal component analysis and Euclidean distance–based sample clustering. Enriched KEGG pathways and gene ontology terms were identified using gene set enrichment analysis (110) or EnrichR (111). Bubble charts representing enrichment analysis were generated using the pathfindR package in R. Venn diagrams of overlaps were generated using an online Venn diagram generator (https://www.meta-chart.com/venn).

Analysis of Data from Publicly Available Databases

Analysis of microarray data from Gene Expression Omnibus (GEO) was done using the NCBI GEO2R online tool for microarray analysis. Quantile normalization was used to process microarray data. Adjusted *P* value calculations were done using the Benjamini–Hochberg option. A *P* value of <0.05 was considered to be statistically significant. Gene essentiality data for cancer cell lines was obtained from the Project Achilles CRISPR-Cas9 screening dataset (https://depmap.org/portal/download/; 2019 Quarter 2 release). Essentiality of individual genes is represented as the inverse of the CERES score for that gene (112). Visualization of gene essentiality data was achieved in Python (version 3.6.4, Anaconda Inc.) using the modules Pandas (v0.23.4) and Seaborn (v0.9.0).

Cell Transfection and Virus Production

293T cells that reach up to 70% confluency were used for transfection using jetPrime reagent followed the recommended protocol (Polyplus). After 48 hours, 293T cells were collected for the subsequent experiment as required. The following short-hairpin RNAs (Sigma-Aldrich, MISSION system) were used:

sh*USP7.1*: 5′-CCGGCCTGGATTTGTGGTTACGTTACTCGAGTAACGTAACCACAAATCCAGGTTTTT-3′,
sh*USP7.2*:5′-CCGGCCAGCTAAGTATCAAAGGAAACTCGAGTTTCCTTTGATACTTAGCTGGTTTTT-3′,
sh*SRSF6.0*:5′-CCGGCGAACAAATGAGGGTGTAATTCTCGAGAATTACACCCTCATTTGTTCGTTTTTG-3′ (TRCN0000231443, NM_006275.4-589s21c1),
sh*SRSF6.1*: 5′-CCGGGCTCCCATTCACATTCTCGAACTCGAGTTCGAGAATGTGAATGGGAGCTTTTT-3′ (TRCN0000006624, NM_006275.4-923s1c1)
and shSRSF6.2: 5′-CCGGGGCAGAAATATTAGGCTTATTCTCGAGAATAAGCCTAATATTTCTGCCTTTTTG-3′(TRCN0000231444,NM_006275.4-673s21c1).
Nonmammalian shRNA control hairpin SHC002 5′-CCGGCAACAAGATGAAGAGCACCAACTCGAGTTGGTGCTCTTCATCTTGTTGTTTTT-3′ was used.

siRNA against *USP7* was a SMARTpool of the following ON-TARGETplus siRNAs: siRNA J-006097-05 (Target Sequence: AAGCGUCCCUUUAGCAUUA), J-006097-06 (GCAUAGUGAUAAACCUGUA), J-006097-07 (UAAGGACCCUGCAAAUUAU), J-006097-08 (GUAAAGAAGUAGACUAUCG). The siRNA control (Silencer negative control #1, 4390843) was purchased from Thermo Fisher Scientific.

For SRSF6 overexpression, the SRSF6 ORF was cloned (using *Bam*HI/*Xho*I) into the Phage vector backbone and the gene is expressed under the CMV promoter. In addition, SRSF6 overexpression vector used in the study was also purchased from Horizon Discovery: *SRSF6*: Precision LentiORF SRSF6, PLOHS_ccbBEn_069 BC006832 BC006832.2 37

The Precision LentiORF USP7 (PLOHS_100066416 BC166690, Horizon Discovery) was used for *USP7* expression in leukemia cells. The control expression vector was Precision LentiORF RFP Positive control E2017121504 (Horizon Discovery).

Inducible short-hairpin RNAs from Horizon Discovery:

sh*UPF1* (TRIPZ Inducible Lentiviral shRNA):
sh*UPF1.1:* RHS4696-200708840 (pTRIPz, TURBORFP, clone ID, V2THS_32895)
sh*UPF1.2:* RHS4696-200681171 (pTRIPz, TURBORFP, Clone Id: V2THS_32893)
sh*USP7* (SMARTvector Inducible Lentiviral):
sh*USP7*: V3SH7669-227599723 (Clone Id: V3IHSHER_7537373)

Control vector for the silencing studies: TRIPZ Inducible Lentiviral Nonsilencing shRNA Control (RHS4743). The Dharmacon TransLentiviral ORF Packaging Kit with calcium phosphate transfection reagent was used for the transfection of all Dharmacon-related constructs following manufacturer's recommendations. Viruses were used to infect T-ALL cells as described previously (42, 69).

Cell Growth and Viability, Apoptosis, Cell-Cycle Analysis, MTT, and Proteasome Activity Assays

To study cell growth, 3,000 cells per well were seeded using a microplate dispenser (MultiFlo, BioTek) in 384-well clear-bottom, black-wall plates (Corning), and drugs were added using the Tecan D300e digital dispenser (Tecan). After 72-hour incubation, AlamarBlue cell viability reagent (Thermo Fisher Scientific) was added and viability was quantified by measuring fluorescence in a plate reader (Tecan Infinite m1000 pro, λ_{ex}: 530 nm; λ_{em}: 590 nm). A total of 500,000 cells were plated in each well of a 24-well plate. For apoptosis analysis, cells were stained with LIVE/DEAD Fixable Near-IR Dead Cell Stain (Life Technologies) according to the manufacturer's protocol, except that cells were stained for 20 minutes at 4°C, prior to staining with PE-conjugated Annexin V (Life Technologies) in Annexin V Binding Buffer (BD Biosciences) according to the manufacturer's instructions. Fortessa cytometer was used for signal detection. For cell-cycle analysis, cells were fixed in 100 μL Fix and Perm Medium A (Life Technologies) for 15 minutes, washed with PBS, and incubated with 0.1% Triton in 1× PBS, supplemented with 1 μg/mL DAPI (Invitrogen) for 6 hours at 4°C. Flow cytometry was performed on an LSR II (BD) and analyses were performed using FlowJo software (Tree Star). Statistical analyses were performed using GraphPad Prism software (GraphPad Software) using Student unpaired, two-sided *t* test or Dunn multiple comparison test.

Cell viability was assessed by MTT ((3-(4,5- dimethylthiazol-2-yl)-2,5-diphenyl tetrazolium bromide) assay. We seeded 100,000 patient cells and 25,000 cells per well in a 96-well plate. At the end of the treatment period, we added 10 μL 5 mg/mL MTT and the cells were incubated for 4 hours followed by the addition of 100 μL of isopropanol:HCl = 500:3.3 mix per well, and the absorbance was measured (560 nm). The growth inhibition 50 (GI_{50}, compound concentration required to inhibit cell growth by 50%) was calculated by plotting the data as a logarithmic function of when viability was 50%. Control cell viability was set to 100%.

For $CD34^+$, M106, M114, and M181 cell growth analysis, we used cytometry and Via Count Kit to remove dead cells (https://www.luminexcorp.com/guava-viacount-reagent-40ml/) and we then gated on single live cells. Staining with hCD45 and hCD7 antibodies was used for the counting of the patient cells.

The Promega chymotrypsin-like kit (G8660) was used to assay proteasomal activity.

Ubiquitination Assays

293T cells were transfected with HA-Ubiquitin or Flag-SRSF6 and treated with either DMSO or 10 μmol/L P5091 USP7 inhibitor for 24 hours. Cells were harvested and lysed and SRSF6 was pulled down using FLAG antibody. Proteins were eluted prior to Western blotting, for detection of ubiquitin levels using HA antibody.

Published OnlineFirst May 22, 2020; DOI: 10.1158/2159-8290.CD-19-1436

Drug Synergism

A total of 3,000 cells per well were seeded using a microplate dispenser (MultiFlo, BioTek) in 384-well clear-bottom, black-wall plates (Corning). Drugs were added using the Tecan D300e digital dispenser (Tecan). After 72-hour incubation, AlamarBlue cell viability reagent (Thermo Fisher Scientific) was added and viability was quantified by measuring fluorescence in a plate reader (Tecan Infinite m1000 pro, λ_{ex}: 530 nm; λ_{em}: 590 nm). Synergy analysis was conducted using SynergyFinder software and the Bliss Independence model (91, 113).

Homology Model Building for PSMG1-201 and PSMG2-202 and Their Validations

The primary amino acid sequences for PSMG1-201 and PMG2-202 having the accession codes NP_003711.1 and NP_982257.1 were obtained from the NCBI database. The PSMG1 protein contains 288 amino acids and PSMG2 is a truncated version of PSMG1 missing a loop of 20 amino acids. We subjected the two query sequences to BLAST/PSI-BLAST engines and obtained homologous (template) structures. Analyzing the template structures, we found that none of them have a sequence identity >40% to both query sequences, which ruled out the possibility of building a single template–based comparative homology model for PSMG1 and PSMG2. Hence, we utilized a multiple template–based homology building tool to generate the models. The different parts of the query sequences were assigned to different template structures to build the models. The Prime 3.1 module implemented in Schrodinger platform (114) was used to build the models. Prime 3.1 is a well-validated protein structure prediction program that integrates comparative modeling and fold recognition into a single interface. The comparative modeling techniques include template identification, alignment, and final model building. Furthermore, it also allows the refinement of the side chains and loops, and minimizes the free energy. On the basis of the template structures, two consensus homology models were built for PSMG1 and PSMG2.

After building models using Prime3.1, we carried out further energy minimization steps using the MacroModel tool available in Schrodinger suite (115). The energy minimized models were then subjected to All-Atoms MolProbity validations (116). The MolProbity validation reveals that both the model structures have <3% clash scores, <5% poor rotamers, and >90% favorable residues in the Ramachandran plot. Finally, no residue was found to have non-favorable dihedral angles or steric collisions. When we superposed both structures, we found structural deviations between the two, as the PSMG2 structure is missing a 20 amino acid loop. The calculated root mean square deviation (RMSD) between the two models was found to be ~ 2.5 Å.

Intravenous and Subcutaneous Xenograft Studies

All mice were housed in a barrier facility, and procedures were performed as approved by the Northwestern University Institutional Animal Care and Use Committee (protocol Ntziachristos #IS00002058 and Mazar #IS00000556).

For CUTLL1 T-ALL intravenous studies, 1 million cells in 100 µL PBS were injected into the tail vein of 8-week-old NOD.Cg-Prkdcscid male mice (#005557, Jackson Laboratories). Body weight and tumor size (via calipers) were measured 3 times per week. Animals were monitored by IVIS every 3 days for luciferase signal detection. IVIS images were taken using the IVIS Spectrum *in vivo* imaging system (PerkinElmer). For statistical analyses, mouse hosts with changes in luciferase values greater or less than the interquartile range of each dataset multiplied by 1.5 were considered outliers and excluded from the study.

Data Availability

The raw files for our proteomics studies are deposited in MassIVE (accession: MSV000084383) https://massive.ucsd.edu/ProteoSAFe/static/massive.jsp. The login information for reviewers at MassIVE is: username: cbk562; password: 3125033711. The raw files for our next-generation sequencing data have been deposited in Gene Expression Omnibus (GEO; GSE139622).

Disclosure of Potential Conflicts of Interest

P. Zhu is an employee with H3 Biomedicine. No potential conflicts of interest were disclosed by the other authors.

Authors' Contributions

Conception and design: Y. Zhou, C. Han, B.T. Guttierrez Diaz, C. Fang, P. Ntziachristos

Development of methodology: Y. Zhou, B.T. Guttierrez Diaz, T. Tabaglio, I. Kandela, I. Aifantis, E. Guccione, P. Ntziachristos

Acquisition of data (provided animals, acquired and managed patients, provided facilities, etc.): C. Han, E. Wang, A.H. Lorch, V. Serafin, B.T. Guttierrez Diaz, J. Calvo, C. Fang, A. Kuchmiy, G. Yacu, S.K. Filip, Q. Jin, E.J. Rendleman, R. Rawat, S. Bresolin, M. Paganin, I. Kandela, Y. Politanska, H. Abdala-Valencia, B. Palhais, P. Van Vlierberghe, T. Taghon, I. Aifantis, Y.A. Goo, A. Heguy, F. Pflumio, B. Accordi, P. Ntziachristos

Analysis and interpretation of data (e.g., statistical analysis, biostatistics, computational analysis): Y. Zhou, A.H. Lorch, V. Serafin, B.-K. Cho, B.T. Guttierrez Diaz, A. Khodadadi-Jamayran, C. Marier, S.K. Filip, D.R. Amici, R. Rawat, S. Bresolin, M. Paganin, C. Zhang, H. Li, M.L. Mendillo, Y.A. Goo, A. Heguy, A. Tsirigos, R.K. Mishra, B. Accordi, P. Ntziachristos

Writing, review, and/or revision of the manuscript: Y. Zhou, C. Han, A.H. Lorch, B.T. Guttierrez Diaz, D.R. Amici, B. Palhais, Y.A. Goo, R.K. Mishra, F. Pflumio, G. Basso, P. Ntziachristos

Administrative, technical, or material support (i.e., reporting or organizing data, constructing databases): Y. Zhou, B.T. Guttierrez Diaz, L. Sun, G. Yacu, Y.-H. Takahashi, P. Zhu, P. Ntziachristos

Study supervision: G. Basso, P. Ntziachristos

Other (designed of all the antisense nucleotides used in the article): K.B. Wee

Other (built and validated the homology models. Carried out the analysis and wrote the *in silico* part in the manuscript): R.K. Mishra

Acknowledgments

The Ntziachristos laboratory is or has been supported by the NCI (R00CA188293 and R01CA248770), the National Science Foundation, the Hartwell Foundation, a Gilead Research Scholarship, the American Society of Hematology, the Leukemia Research Foundation, the St. Baldrick's Foundation, the H Foundation, the Gabrielle's Angel Foundation, the Elsa Pardee Foundation, and the Zell Foundation. B.T. Guttierrez Diaz has been supported by the Fulbright Foundation and The Graduate School of Northwestern University. D.R. Amici was supported by 5T32GM008152-33. Proteomics services were performed by the Northwestern Proteomics Core Facility, supported by NCI CCSG P30 CA060553 awarded to the Robert H. Lurie Comprehensive Cancer Center, instrumentation award (S10OD025194) from NIH Office of Director, and the National Resource for Translational and Developmental Proteomics supported by P41 GM108569. A. Tsirigos is supported by the American Cancer Society (RSG-15-189-01-RMC), St. Baldrick's foundation (581357) and NCI/NIH P01CA229086-01A1. We thank the NYU Langone Genome Technology Center (GTC) for PacBio Sequel sequencing, acquired with the Shared Instrumentation Grant 1S10OD023423-01 from NIH. We also thank the Applied Bioinformatics Laboratories (ABL) for providing bioinformatics support and helping with the analysis and interpretation of the data. GTC and ABL are shared resources partially

supported by the NYU Cancer Center Support Grant P30CA016087 at the Laura and Isaac Perlmutter Cancer Center. This work has used computing resources at the NYU School of Medicine High Performance Computing Facility. We want to thank Dr. Issam Ben Sahra and laboratory and the Department of Biochemistry and Molecular Genetics for helping with reagents and equipment used in the study as well as all the members of the Ntziachristos laboratory for their comments and critical review of the manuscript.

The costs of publication of this article were defrayed in part by the payment of page charges. This article must therefore be hereby marked *advertisement* in accordance with 18 U.S.C. Section 1734 solely to indicate this fact.

Received December 10, 2019; revised April 21, 2020; accepted May 19, 2020; published first May 22, 2020.

REFERENCES

1. Wang ET, Sandberg R, Luo S, Khrebtukova I, Zhang L, Mayr C, et al. Alternative isoform regulation in human tissue transcriptomes. Nature 2008;456:470–6.
2. Kim E, Ilagan JO, Liang Y, Daubner GM, Lee SC-W, Ramakrishnan A, et al. SRSF2 mutations contribute to myelodysplasia by mutant-specific effects on exon recognition. Cancer Cell 2015;27:617–30.
3. Lee SC, Dvinge H, Kim E, Cho H, Micol J-B, Chung YR, et al. Modulation of splicing catalysis for therapeutic targeting of leukemia with mutations in genes encoding spliceosomal proteins. Nat Med 2016;22:672–8.
4. Ntziachristos P, Abdel-Wahab O, Aifantis I. Emerging concepts of epigenetic dysregulation in hematological malignancies. Nat Immunol 2016;17:1016–24.
5. Dvinge H, Kim E, Abdel-Wahab O, Bradley RK. RNA splicing factors as oncoproteins and tumour suppressors. Nat Rev Cancer 2016;16:413–30.
6. Inoue D, Abdel-Wahab O. Modeling SF3B1 mutations in cancer: advances, challenges, and opportunities. Cancer Cell 2016;30:371–3.
7. Shirai CL, Ley JN, White BS, Kim S, Tibbitts J, Shao J, et al. Mutant U2AF1 expression alters hematopoiesis and pre-mRNA splicing in vivo. Cancer Cell 2015;27:631–43.
8. Yoshimi A, Abdel-Wahab O. Molecular pathways: understanding and targeting mutant spliceosomal proteins. Clin Cancer Res 2017;23:336–41.
9. Yoshimi A, Lin K-T, Wiseman DH, Rahman MA, Pastore A, Wang B, et al. Coordinated alterations in RNA splicing and epigenetic regulation drive leukaemogenesis. Nature 2019;574:273–7.
10. Inoue D, Chew G-L, Liu B, Michel BC, Pangallo J, D'Avino AR, et al. Spliceosomal disruption of the non-canonical BAF complex in cancer. Nature 2019;574:432–6.
11. Papaemmanuil E, Cazzola M, Boultwood J, Malcovati L, Vyas P, Bowen D, et al. Somatic SF3B1 mutation in myelodysplasia with ring sideroblasts. N Engl J Med 2011;365:1384–95.
12. Rossi D, Bruscaggin A, Spina V, Rasi S, Khiabanian H, Messina M, et al. Mutations of the SF3B1 splicing factor in chronic lymphocytic leukemia: association with progression and fludarabine-refractoriness. Blood 2011;118:6904–8.
13. Yoshida K, Sanada M, Shiraishi Y, Nowak D, Nagata Y, Yamamoto R, et al. Frequent pathway mutations of splicing machinery in myelodysplasia. Nature 2011;478:64–9.
14. Lee SC-W, North K, Kim E, Jang E, Obeng E, Lu SX, et al. Synthetic lethal and convergent biological effects of cancer-associated spliceosomal gene mutations. Cancer Cell 2018;34:225–41.
15. Shuai S, Suzuki H, Diaz-Navarro A, Nadeu F, Kumar SA, Gutierrez-Fernandez A, et al. The U1 spliceosomal RNA is recurrently mutated in multiple cancers. Nature 2019;574:712–6.
16. Karni R, de Stanchina E, Lowe SW, Sinha R, Mu D, Krainer AR. The gene encoding the splicing factor SF2/ASF is a proto-oncogene. Nat Struct Mol Biol 2007;14:185–93.
17. Anczuków O, Rosenberg AZ, Akerman M, Das S, Zhan L, Karni R, et al. The splicing factor SRSF1 regulates apoptosis and proliferation to promote mammary epithelial cell transformation. Nat Struct Mol Biol 2012;19:220–8.
18. Das S, Anczukow O, Akerman M, Krainer AR. Oncogenic splicing factor SRSF1 is a critical transcriptional target of MYC. Cell Rep 2012;1:110–7.
19. Anczuków O, Akerman M, Cléry A, Wu J, Shen C, Shirole NH, et al. SRSF1-regulated alternative splicing in breast cancer. Mol Cell 2015;60:105–17.
20. Cohen-Eliav M, Golan-Gerstl R, Siegfried Z, Andersen CL, Thorsen K, Ørntoft TF, et al. The splicing factor SRSF6 is amplified and is an oncoprotein in lung and colon cancers. J Pathol 2013;229:630–9.
21. Jensen MA, Wilkinson JE, Krainer AR. Splicing factor SRSF6 promotes hyperplasia of sensitized skin. Nat Struct Mol Biol 2014;21:189–97.
22. He X, Ee PL, Coon JS, Beck WT. Alternative splicing of the multidrug resistance protein 1/ATP binding cassette transporter subfamily gene in ovarian cancer creates functional splice variants and is associated with increased expression of the splicing factors PTB and SRp20. Clin Cancer Res 2004;10:4652–60.
23. Jia R, Li C, McCoy JP, Deng CX, Zheng ZM. SRp20 is a proto-oncogene critical for cell proliferation and tumor induction and maintenance. Int J Biol Sci 2010;6:806–26.
24. Iborra S, Hirschfeld M, Jaeger M, zur Hausen A, Braicu I, Sehouli J, et al. Alterations in expression pattern of splicing factors in epithelial ovarian cancer and its clinical impact. Int J Gynecol Cancer 2013;23:990–6.
25. Ghigna C, Giordano S, Shen H, Benvenuto F, Castiglioni F, Comoglio PM, et al. Cell motility is controlled by SF2/ASF through alternative splicing of the Ron protooncogene. Mol Cell 2005;20:881–90.
26. Hunger SP, Mullighan CG. Acute lymphoblastic leukemia in children. N Engl J Med 2015;373:1541–52.
27. Pui CH, Relling MV, Downing JR. Acute lymphoblastic leukemia. N Engl J Med 2004;350:1535–48.
28. Pui CH, Mullighan CG, Evans WE, Relling MV. Pediatric acute lymphoblastic leukemia: where are we going and how do we get there? Blood 2012;120:1165–74.
29. Pui CH, Evans WE. Treatment of acute lymphoblastic leukemia. N Engl J Med 2006;354:166–78.
30. Aifantis I, Raetz E, Buonamici S. Molecular pathogenesis of T-cell leukaemia and lymphoma. Nat Rev Immunol 2008;8:380–90.
31. Pui CH, Robison LL, Look AT. Acute lymphoblastic leukaemia. Lancet 2008;371:1030–43.
32. Shah A, Coleman MP. Increasing incidence of childhood leukaemia: a controversy re-examined. Br J Cancer 2007;97:1009–12.
33. Haydu JE, Ferrando AA. Early T-cell precursor acute lymphoblastic leukaemia. Curr Opin Hematol 2013;20:369–73.
34. Coustan-Smith E, Mullighan CG, Onciu M, Behm FG, Raimondi SC, Pei D, et al. Early T-cell precursor leukaemia: a subtype of very high-risk acute lymphoblastic leukaemia. Lancet Oncol 2009;10:147–56.
35. Weng AP, Ferrando AA, Lee W, Morris JP IV, Silverman LB, Sanchez-Irizarry C, et al. Activating mutations of NOTCH1 in human T cell acute lymphoblastic leukemia. Science 2004;306:269–71.
36. Real PJ, Tosello V, Palomero T, Castillo M, Hernando E, de Stanchina E, et al. Gamma-secretase inhibitors reverse glucocorticoid resistance in T cell acute lymphoblastic leukemia. Nat Med 2009;15:50–8.
37. Tosello V, Mansour MR, Barnes K, Paganin M, Sulis ML, Jenkinson S, et al. WT1 mutations in T-ALL. Blood 2009;114:1038–45.
38. De Keersmaecker K, Ferrando AA. TLX1-induced T-cell acute lymphoblastic leukemia. Clin Cancer Res 2011;17:6381–6.
39. Zenatti PP, Ribeiro D, Li W, Zuurbier L, Silva MC, Paganin M, et al. Oncogenic IL7R gain-of-function mutations in childhood T-cell acute lymphoblastic leukemia. Nat Genet 2011;43:932–9.
40. Ntziachristos P, Tsirigos A, Vlierberghe PV, Nedjic J, Trimarchi T, Flaherty MS, et al. Genetic inactivation of the polycomb repressive complex 2 in T cell acute lymphoblastic leukemia. Nat Med 2012;18:298–301.
41. Ntziachristos P, Tsirigos A, Welstead GG, Trimarchi T, Bakogianni S, Xu L, et al. Contrasting roles of histone 3 lysine 27 demethylases in acute lymphoblastic leukaemia. Nature 2014;514:513–7.

Published OnlineFirst May 22, 2020; DOI: 10.1158/2159-8290.CD-19-1436

42. Trimarchi T, Bilal E, Ntziachristos P, Fabbri G, Dalla-Favera R, Tsirigos A, et al. Genome-wide mapping and characterization of Notch-regulated long noncoding RNAs in acute leukemia. Cell 2014;158:593–606.
43. Buonamici S, Trimarchi T, Ruocco MG, Reavie L, Cathelin S, Mar BG, et al. CCR7 signalling as an essential regulator of CNS infiltration in T-cell leukaemia. Nature 2009;459:1000–4.
44. Mullighan CG, Downing JR. Global genomic characterization of acute lymphoblastic leukemia. Semin Hematol 2009;46:3–15.
45. Zhang J, Ding L, Holmfeldt L, Wu G, Heatley SL, Payne-Turner D, et al. The genetic basis of early T-cell precursor acute lymphoblastic leukaemia. Nature 2012;481:157–63.
46. Roberts KG, Mullighan CG. Genomics in acute lymphoblastic leukaemia: insights and treatment implications. Nat Rev Clin Oncol 2015;12:344–57.
47. Liu Y, Easton J, Shao Y, Maciaszek J, Wang Z, Wilkinson MR, et al. The genomic landscape of pediatric and young adult T-lineage acute lymphoblastic leukemia. Nat Genet 2017;49:1211–8.
48. Robinson MD, McCarthy DJ, Smyth GK. edgeR: a Bioconductor package for differential expression analysis of digital gene expression data. Bioinformatics 2010;26:139–40.
49. Shen S, Park JW, Lu Z-X, Lin L, Henry MD, Wu YN, et al. rMATS: robust and flexible detection of differential alternative splicing from replicate RNA-Seq data. Proc Natl Acad Sci U S A 2014;111:E5593–601.
50. Uppal S, Gegonne A, Chen Q, Thompson PS, Cheng D, Mu J, et al. The bromodomain protein 4 contributes to the regulation of alternative splicing. Cell Rep 2019;29:2450–60.
51. Lareau LF, Brenner SE. Regulation of splicing factors by alternative splicing and NMD is conserved between kingdoms yet evolutionarily flexible. Mol Biol Evol 2015;32:1072–9.
52. Lareau LF, Inada M, Green RE, Wengrod JC, Brenner SE. Unproductive splicing of SR genes associated with highly conserved and ultraconserved DNA elements. Nature 2007;446:926–9.
53. Park JW, Jung S, Rouchka EC, Tseng YT, Xing Y. rMAPS: RNA map analysis and plotting server for alternative exon regulation. Nucleic Acids Res 2016;44:W333–8.
54. Tsherniak A, Vazquez F, Montgomery PG, Weir BA, Kryukov G, Cowley GS, et al. Defining a cancer dependency map. Cell 2017;170:564–76.
55. Gerstberger S, Hafner M, Tuschl T. A census of human RNA-binding proteins. Nat Rev Genet 2014;15:829–45.
56. Lunde BM, Moore C, Varani G. RNA-binding proteins: modular design for efficient function. Nat Rev Mol Cell Biol 2007;8:479–90.
57. Wang E, Lu SX, Pastore A, Chen X, Imig J, Chun-Wei Lee S, et al. Targeting an RNA-binding protein network in acute myeloid leukemia. Cancer Cell 2019;35:369–84.
58. Shalem O, Sanjana NE, Hartenian E, Shi X, Scott DA, Mikkelsen TS, et al. Genome-scale CRISPR-Cas9 knockout screening in human cells. Science 2014;343:84–7.
59. Wang T, Yu H, Hughes NW, Liu B, Kendirli A, Klein K, et al. Gene essentiality profiling reveals gene networks and synthetic lethal interactions with oncogenic Ras. Cell 2017;168:890–903.
60. Shi J, Wang E, Milazzo JP, Wang Z, Kinney JB, Vakoc CR. Discovery of cancer drug targets by CRISPR-Cas9 screening of protein domains. Nat Biotechnol 2015;33:661–7.
61. Hart T, Chandrashekhar M, Aregger M, Steinhart Z, Brown KR, MacLeod G, et al. High-resolution CRISPR screens reveal fitness genes and genotype-specific cancer liabilities. Cell 2015;163:1515–26.
62. Neumann M, Vosberg S, Schlee C, Heesch S, Schwartz S, Gökbuget N, et al. Mutational spectrum of adult T-ALL. Oncotarget 2015;6:2754–66.
63. Puente XS, Pinyol M, Quesada V, Conde L, Ordóñez GR, Villamor N, et al. Whole-genome sequencing identifies recurrent mutations in chronic lymphocytic leukaemia. Nature 2011;475:101–5.
64. Malcovati L, Papaemmanuil E, Bowen DT, Boultwood J, Della Porta MG, Pascutto C, et al. Clinical significance of SF3B1 mutations in myelodysplastic syndromes and myelodysplastic/myeloproliferative neoplasms. Blood 2011;118:6239–46.
65. Van Vlierberghe P, Ambesi-Impiombato A, Perez-Garcia A, Haydu JE, Rigo I, Hadler M, et al. ETV6 mutations in early immature human T cell leukemias. J Exp Med 2011;208:2571–9.
66. Koh CM, Bezzi M, Low DHP, Ang WX, Teo SX, Gay FPH, et al. MYC regulates the core pre-mRNA splicing machinery as an essential step in lymphomagenesis. Nature 2015;523:96–100.
67. Hsu TY-T, Simon LM, Neill NJ, Marcotte R, Sayad A, Bland CS, et al. The spliceosome is a therapeutic vulnerability in MYC-driven cancer. Nature 2015;525:384–8.
68. Su H, Hu J, Huang L, Yang Y, Thenoz M, Kuchmiy A, et al. SHQ1 regulation of RNA splicing is required for T-lymphoblastic leukemia cell survival. Nat Commun 2018;9:4281.
69. Jin Q, Martinez CA, Arcipowski KM, Zhu Y, Gutierrez-Diaz BT, Wang KK, et al. USP7 Cooperates with NOTCH1 to drive the oncogenic transcriptional program in T-cell leukemia. Clin Cancer Res 2019;25:222–39.
70. Rawat R, Starczynowski DT, Ntziachristos P. Nuclear deubiquitination in the spotlight: the multifaceted nature of USP7 biology in disease. Curr Opin Cell Biol 2019;58:85–94.
71. Kumar D, Das M, Sauceda C, Ellies LG, Kuo K, Parwal P, et al. Degradation of splicing factor SRSF3 contributes to progressive liver disease. J Clin Invest 2019;130:4477–91.
72. Jayabalan AK, Sanchez A, Park RY, Yoon SP, Kang G-Y, Baek J-H, et al. NEDDylation promotes stress granule assembly. Nat Commun 2016;7:12125.
73. Maertens GN, El Messaoudi-Aubert S, Elderkin S, Hiom K, Peters G. Ubiquitin-specific proteases 7 and 11 modulate Polycomb regulation of the INK4a tumour suppressor. EMBO J 2010;29:2553–65.
74. Georges A, Marcon E, Greenblatt J, Frappier L. Identification and characterization of USP7 targets in cancer cells. Sci Rep 2018;8:15833.
75. Sowa ME, Bennett EJ, Gygi SP, Harper JW. Defining the human deubiquitinating enzyme interaction landscape. Cell 2009;138:389–403.
76. Palazón-Riquelme P, Worboys JD, Green J, Valera A, Martín-Sánchez F, Pellegrini C, et al. USP7 and USP47 deubiquitinases regulate NLRP3 inflammasome activation. EMBO Rep 2018;19:e44766.
77. Chauhan D, Tian Z, Nicholson B, Kumar KGS, Zhou B, Carrasco R, et al. A small molecule inhibitor of ubiquitin-specific protease-7 induces apoptosis in multiple myeloma cells and overcomes bortezomib resistance. Cancer Cell 2012;22:345–58.
78. Altun M, Kramer HB, Willems LI, McDermott JL, Leach CA, Goldenberg SJ, et al. Activity-based chemical proteomics accelerates inhibitor development for deubiquitylating enzymes. Chem Biol 2011;18:1401–12.
79. Tzelepis K, De Braekeleer E, Aspris D, Barbieri I, Vijayabaskar MS, Liu W-H, et al. SRPK1 maintains acute myeloid leukemia through effects on isoform usage of epigenetic regulators including BRD4. Nat Commun 2018;9:5378.
80. Seiler M, Yoshimi A, Darman R, Chan B, Keaney G, Thomas M, et al. H3B-8800, an orally available small-molecule splicing modulator, induces lethality in spliceosome-mutant cancers. Nat Med 2018;24:497–504.
81. Aird D, Teng T, Huang C-L, Pazolli E, Banka D, Cheung-Ong K, et al. Sensitivity to splicing modulation of BCL2 family genes defines cancer therapeutic strategies for splicing modulators. Nat Commun 2019;10:137.
82. Hirano Y, Hendil KB, Yashiroda H, Iemura S-I, Nagane R, Hioki Y, et al. A heterodimeric complex that promotes the assembly of mammalian 20S proteasomes. Nature 2005;437:1381–5.
83. Sasaki K, Hamazaki J, Koike M, Hirano Y, Komatsu M, Uchiyama Y, et al. PAC1 gene knockout reveals an essential role of chaperone-mediated 20S proteasome biogenesis and latent 20S proteasomes in cellular homeostasis. Mol Cell Biol 2010;30:3864–74.
84. Wani PS, Rowland MA, Ondracek A, Deeds EJ, Roelofs J. Maturation of the proteasome core particle induces an affinity switch that controls regulatory particle association. Nat Commun 2015;6:6384.
85. Trapnell C, Williams BA, Pertea G, Mortazavi A, Kwan G, van Baren MJ, et al. Transcript assembly and quantification by RNA-Seq reveals unannotated transcripts and isoform switching during cell differentiation. Nat Biotechnol 2010;28:511–5.
86. Anders S, Reyes A, Huber W. Detecting differential usage of exons from RNA-seq data. Genome Res 2012;22:2008–17.
87. Koyama D, Kikuchi J, Hiraoka N, Wada T, Kurosawa H, Chiba S, et al. Proteasome inhibitors exert cytotoxicity and increase

Published OnlineFirst May 22, 2020; DOI: 10.1158/2159-8290.CD-19-1436

chemosensitivity via transcriptional repression of Notch1 in T-cell acute lymphoblastic leukemia. Leukemia 2014;28:1216–26.
88. Takahashi K, Inukai T, Imamura T, Yano M, Tomoyasu C, Lucas DM, et al. Anti-leukemic activity of bortezomib and carfilzomib on B-cell precursor ALL cell lines. PLoS One 2017;12:e0188680.
89. Boccadoro M, Morgan G, Cavenagh J. Preclinical evaluation of the proteasome inhibitor bortezomib in cancer therapy. Cancer Cell Int 2005;5:18.
90. Satou Y, Nosaka K, Koya Y, Yasunaga J-I, Toyokuni S, Matsuoka M. Proteasome inhibitor, bortezomib, potently inhibits the growth of adult T-cell leukemia cells both in vivo and in vitro. Leukemia 2004;18:1357–63.
91. Foucquier J, Guedj M. Analysis of drug combinations: current methodological landscape. Pharmacol Res Perspect 2015;3:e00149.
92. Black KL, Naqvi AS, Asnani M, Hayer KE, Yang SY, Gillespie E, et al. Aberrant splicing in B-cell acute lymphoblastic leukemia. Nucleic Acids Res 2018;46:11357–69.
93. Kahles A, Lehmann K-V, Toussaint NC, Hüser M, Stark SG, Sachsenberg T, et al. Comprehensive analysis of alternative splicing across tumors from 8,705 patients. Cancer Cell 2018;34:211–24.
94. Aubol BE, Chakrabarti S, Ngo J, Shaffer J, Nolen B, Fu X-D, et al. Processive phosphorylation of alternative splicing factor/splicing factor 2. Proc Natl Acad Sci U S A 2003;100:12601–6.
95. Braun CJ, Stanciu M, Boutz PL, Patterson JC, Calligaris D, Higuchi F, et al. Coordinated splicing of regulatory detained introns within oncogenic transcripts creates an exploitable vulnerability in malignant glioma. Cancer Cell 2017;32:411–26.
96. Bezzi M, Teo SX, Muller J, Mok WC, Sahu SK, Vardy LA, et al. Regulation of constitutive and alternative splicing by PRMT5 reveals a role for Mdm4 pre-mRNA in sensing defects in the spliceosomal machinery. Genes Dev 2013;27:1903–16.
97. Fong JY, Pignata L, Goy PA, Kawabata KC, Lee SC, Koh CM, et al. Therapeutic targeting of RNA splicing catalysis through inhibition of protein arginine methylation. Cancer Cell 2019;36:194–209.
98. Stamm S. Regulation of alternative splicing by reversible protein phosphorylation. J Biol Chem 2008;283:1223–7.
99. Zhang L, Tran N-T, Su H, Wang R, Lu Y, Tang H, et al. Cross-talk between PRMT1-mediated methylation and ubiquitylation on RBM15 controls RNA splicing. Elife 2015;4:e07938.
100. Moulton VR, Gillooly AR, Tsokos GC. Ubiquitination regulates expression of the serine/arginine-rich splicing factor 1 (SRSF1) in normal and systemic lupus erythematosus (SLE) T cells. J Biol Chem 2014;289:4126–34.
101. Bellare P, Small EC, Huang X, Wohlschlegel JA, Staley JP, Sontheimer EJ. A role for ubiquitin in the spliceosome assembly pathway. Nat Struct Mol Biol 2008;15:444–51.
102. Bellare P, Kutach AK, Rines AK, Guthrie C, Sontheimer EJ. Ubiquitin binding by a variant Jab1/MPN domain in the essential pre-mRNA splicing factor Prp8p. RNA 2006;12:292–302.
103. Fang J, Bolanos LC, Choi K, Liu X, Christie S, Akunuru S, et al. Ubiquitination of hnRNPA1 by TRAF6 links chronic innate immune signaling with myelodysplasia. Nat Immunol 2017;18:236–45.
104. Paolella BR, Gibson WJ, Urbanski LM, Alberta JA, Zack TI, Bandopadhayay P, et al. Copy-number and gene dependency analysis reveals partial copy loss of wild-type SF3B1 as a novel cancer vulnerability. Elife 2017;6:e23268.
105. Steensma DP, Wermke M, Klimek VM, Greenberg PL, Font P, Komrokji RS, et al. Results of a clinical trial of H3B-8800, a splicing modulator, in patients with myelodysplastic syndromes (MDS), acute myeloid leukemia (AML) or chronic myelomonocytic leukemia (CMML). Blood 2019;134:673.
106. Yatim A, Benne C, Sobhian B, Laurent-Chabalier S, Deas O, Judde J-G, et al. NOTCH1 nuclear interactome reveals key regulators of its transcriptional activity and oncogenic function. Mol Cell 2012;48:445–58.
107. Kourtis N, Lazaris C, Hockemeyer K, Balandrán JC, Jimenez AR, Mullenders J, et al. Oncogenic hijacking of the stress response machinery in T cell acute lymphoblastic leukemia. Nat Med 2018;24:1157–66.
108. Milani G, Rebora P, Accordi B, Galla L, Bresolin S, Cazzaniga G, et al. Low PKCalpha expression within the MRD-HR stratum defines a new subgroup of childhood T-ALL with very poor outcome. Oncotarget 2014;5:5234–45.
109. Serafin V, Lissandron V, Buldini B, Bresolin S, Paganin M, Grillo F, et al. Phosphoproteomic analysis reveals hyperactivation of mTOR/STAT3 and LCK/Calcineurin axes in pediatric early T-cell precursor ALL. Leukemia 2017;31:1007–11.
110. Subramanian A, Tamayo P, Mootha VK, Mukherjee S, Ebert BL, Gillette MA, et al. Gene set enrichment analysis: a knowledge-based approach for interpreting genome-wide expression profiles. Proc Natl Acad Sci U S A 2005;102:15545–50.
111. Chen EY, Tan CM, Kou Y, Duan Q, Wang Z, Meirelles G, et al. Enrichr: interactive and collaborative HTML5 gene list enrichment analysis tool. BMC Bioinformatics 2013;14:128.
112. Meyers RM, Bryan JG, McFarland JM, Weir BA, Sizemore AE, Xu H, et al. Computational correction of copy number effect improves specificity of CRISPR-Cas9 essentiality screens in cancer cells. Nat Genet 2017;49:1779–84.
113. Ianevski A, He L, Aittokallio T, Tang J. SynergyFinder: a web application for analyzing drug combination dose-response matrix data. Bioinformatics 2017;33:2413–5.
114. Farid R, Day T, Friesner RA, Pearlstein RA. New insights about HERG blockade obtained from protein modeling, potential energy mapping, and docking studies. Bioorg Med Chem 2006;14:3160–73.
115. Bhachoo J, Beuming T. Investigating protein-peptide interactions using the schrodinger computational suite. Methods Mol Biol 2017;1561:235–54.
116. Chen VB, Arendall WB, Headd JJ, Keedy DA, Immormino RM, Kapral GJ, et al. MolProbity: all-atom structure validation for macromolecular crystallography. Acta Crystallogr D Biol Crystallogr 2010;66:12–21.

Published OnlineFirst May 22, 2020; DOI: 10.1158/2159-8290.CD-19-1436

AACR American Association for Cancer Research

CANCER DISCOVERY

Posttranslational Regulation of the Exon Skipping Machinery Controls Aberrant Splicing in Leukemia

Yalu Zhou, Cuijuan Han, Eric Wang, et al.

Cancer Discov Published OnlineFirst May 22, 2020.